Article

Not peer-reviewed version

Novel mitochondria-targeted amphiphilic aminophosphonium salts and lipids nanoparticles: synthesis, antitumor activity and toxicity

Vladimir F. Mironov *, Mudaris N. Dimukhametov, Andrey V. Nemtarev, Tatiana N. Pashirova, Olga V. Tsepaeva, Alexandra D. Voloshina, Alexandra B. Vyshtakalyuk, Igor A. Litvinov, Anna P. Lyubina, Anastasiia S. Sapunova, Dinara F. Abramova, Vladimir V. Zobov

Posted Date: 22 September 2023

doi: 10.20944/preprints202309.1553.v1

Keywords: aminophosphonium salt; liposome; solid lipid nanoparticle; anticancer activity; apoptosis; antimicrobial activity; hemolytic activity; acute toxicity.

Article

Novel Mitochondria-Targeted Amphiphilic Aminophosphonium Salts and Lipids Nanoparticles: Synthesis, Antitumor Activity and Toxicity

Vladimir F. Mironov [1,2,*], Mudaris N. Dimukhametov [1], Andrey V. Nemtarev [1,2], Tatiana N. Pashirova [1], Olga V. Tsepaeva [1], Alexandra D. Voloshina [1], Alexandra B. Vyshtakalyuk [1], Igor A. Litvinov [1], Anna P. Lyubina [1], Anastasiya S. Sapunova [1], Dinara F. Abramova [1] and Vladimir V. Zobov [1]

[1] Arbuzov Institute of Organic and Physical Chemistry, FRC Kazan Scientific Center of RAS, 8 Arbuzov St., 420088 Kazan, Russian Federation; mironov@iopc.ru (V.F.M.); a.nemtarev@mail.ru (A.V.N.); tatyana_pashirova@mail.ru (T.N.P.)

[2] Alexander Butlerov Institute of Chemistry, Kazan (Volga Region) Federal University, 18 Kremlevskaya St., 420008 Kazan, Russian Federation

* Correspondence: mironov@iopc.ru

Abstract: The creation of mitochondria-targeted vector systems is a new tool for the treatment of socially significant diseases. Phosphonium groups provide targeted delivery of drugs through biological barriers to organelles. For this purpose, a new class of alkyl(diethylAmino)(Phenyl) Phosphonium halides (APP) containing one, two, or three diethylamino groups were obtained by the reaction of alkyl iodides (bromides) with (diethylamino)(phenyl)phosphines under mild conditions (20 °C) and high yields (93-98%). The structure of APP was established by NMR and XRD. A high in vitro cytotoxicity of APP against M-Hela, HuTu 80, PC3, DU-145, PANC-1 and MCF-7 lines was found. Selectivity index are in the range of 0.06-4.0 μM (SI 17-277) for the most active APP. The effect of APP on cancer cells are characterized by hyperproduction of ROS and depolarization of the mitochondrial membrane. APP induce apoptosis proceeding along the mitochondrial pathway. Incorporation of APP into lipid systems (liposomes and solid lipid nanoparticles) improve the cytotoxicity toward tumor cells and decrease the toxicity against normal cell lines. APP exhibit a high selective activity against the Gram-positive bacteria *S. aureus 209P*, *B. segeus 8035*, including methicillin-resistant *S. aureus* (*MRSA-1, MRSA-2*), comparable to the activity of fluoroquinolone antibiotic norfloxacin. A moderate in vivo toxicity in CD-1 mice was established for the lead APP.

Keywords: aminophosphonium salt; liposome; solid lipid nanoparticle; anticancer activity; apoptosis; antimicrobial activity; hemolytic activity; acute toxicity

1. Introduction

To date, cardiovascular, neurodegenerative, tumor diseases, as well as chronic inflammation occupy one of the leading positions in the cause of death of people around the world. The occurrence of these pathologies and their progression are largely associated with mitochondrial dysfunction [1–9]. Mitochondria, being one of the most important organelles of eukaryotic cells, are involved in the transformation of energy-rich molecules, such as carbohydrates, lipids and amino acids, into a macroergic ATP molecule through oxidative phosphorylation (OXPHOS) [10]. They play a key role in many metabolic processes, such as the tricarboxylic acid cycle, oxidative decarboxylation of pyruvate by the pyruvate dehydrogenase complex [11], in the biosynthesis of iron-sulfur enzymes [12] and steroids [13]. Reactive oxygen (ROS) and nitrogen (RNS) species arising during oxidative phosphorylation play a major role in redox cell signaling under hypoxia, cell differentiation and innate immunity [14,15]. Mitochondria participate in the ornithine cycle (urea cycle) [16] and are responsible for calcium homeostasis [17]. The mitochondrial permeability transition (mPT) is a sensor of stress and damage, and mitochondria play a central role in cell death – apoptosis [18,19], ferroptosis [20–22] and necrosis [23,24]. Taking into account the key role that mitochondria play in

regulating cell life and death, in recent decades, a mitochondrial-oriented approach to the treatment of metabolic and degenerative diseases, consisting in the use of molecules containing mitochondria-specific compounds that selectively accumulate in mitochondria, has been intensively studied [25]. Especially effective here are delocalized lipophilic triphenylphosphonium (TPP) cations, which have been used to deliver a wide range of medicinal, diagnostic cargoes and analytical probes to mitochondria [26–28]. The penetration of such cations through the hydrophobic layer of the lipid membrane is often the limiting stage of their accumulation in cells and mitochondria. In tumor cells characterized by hyperpolarized (in comparison with normal cells) mitochondrial membrane (Ψ_{IM} ~ –220 mV) [29], in the presence of sufficient oxygen, stable aerobic glycolysis (Warburg effect) is observed [30,31]. The difference in transmembrane mitochondrial potentials in tumor and normal cells ($\Delta\Psi$ about 60 mV) leads to multiple (up to 1×10^3 times) accumulation of the lipophilic cations in tumor cells, thereby conferring the property of selectivity [32]. It is also known that some lipophilic cations cause a strong separation of respiration and oxidative phosphorylation, depolarizing the mitochondria of tumor cells and thereby initiating apoptosis [33].

In TPP-conjugates, the combination of a therapeutic or diagnostic load with a phosphonic group is carried out, as a rule, by means of a covalent bond through a linker, the nature of which is given a great attention. Thus, data on the influence of the linker nature have been presented in many works [34–41]. There is a report on the effect of the R substituent in $R–P^+Ph_3$ salts on their biological properties [42]. At the same time, there are a few publications in which the nature of substituents in aryl fragments of lipophilic $R–P^+Ar_3$ cations themselves has been demonstrated to have a great influence on their biological, including cytostatic properties [43–46]. Thus, it has been shown that the structural modification of the TPP^+ phenyl rings, which reduces the electron density on the phosphorus atom, can lead to the disappearance of the uncoupling activity compared to the original TPP^+ fragment [43]. However, a change in the structure of the aryl substituent in the $Ar_3P^+–R$ cation does not have a negative effect on the delivery of cargo to the mitochondria [45].

A number of studies have been carried out to clarify the role of delocalization of the charge of lipophilic cations in the efficiency of their penetration through lipid membranes and it has been shown that both cyclohexyl and aryl fragments are not necessary for the effective penetration of lipophilic cations through them [47,48]. It is shown that the presence of halide or methyl substituents in the phenyl ring of the triphenylphosphonium cation can accelerate the penetration of such hydrophobic cations through lipid membranes and thereby enhance their effect in those biological systems where penetration is a limiting stage. It turned out that for some analogues, an increase in hydrophobicity correlates with an increase in the penetration rate constant, but there is no complete accordance [49].

The creation of the nanotherapeutic drugs aimed at certain cellular organelles is based on the use of such advantages of nanomedicine as [50] (i) molecular therapy, (ii) an increased ratio of the surface area of nanoparticles (NPS) to their volume, which allows to increase efficiency and safety when administered at lower doses, (iii) a possibility of the functionalization of the NPS surface to avoid an immune response, (iv) effective accumulation of NPS through the vascular network. These advantages create certain prospects for cancer therapy in the future [51–54]. Organelle-directed delivery systems will be able to solve such major problems as a high toxicity of antitumor drugs and multiple drug resistance. In addition, colloidal carriers are able to improve the solubility of medicinal substances, prevent degradation, prolong their action, and i.e., generally increase their effectiveness. Natural and biodegradable nanomaterials are the most promising for clinical use [55–57]. The successful application of lipid nanoparticles for cancer therapy is presented in [58–62]. From a wide range of mitochondrial-directed NPS, the attention of our group is attracted by the lipid nanosystems functionalized with triphenylphosphonium fragments [63,64].

$Ar_3P^+–R$ salts, despite their high efficiency in the targeted delivery to the tumor cells, often show a high toxicity in in vitro experiments with respect to the normal cells and do not undergo a biodegradation, which can become a problem for removing such substances from the body. In this regard, the search for effective phosphorus-containing vector systems is currently intensively underway. Also, despite numerous studies in this field, the question remains open about the effect

Preprints (www.preprints.org) | NOT PEER-REVIEWED | Posted: 22 September 2023 doi:10.20944/preprints202309.1553.v1

of the positive charge delocalization degree in triaryl-phosphonium cations on its ability to penetrate mitochondrial membranes and on subsequent biological properties. It is known that heteroatoms more effectively stabilize the positive charge on carbenium ions, due to donating a lone pair of electrons (LPE) to the corresponding vacant orbital of electron-deficient carbon [65].

It seemed very interesting to find out how the introduction of the heteroatoms with LPE to the phosphorus atom would affect the transport and biological properties of the phosphonium cation, which should more effectively extinguish a positive charge on the phosphorus atom than aryl groups with substituents of any nature. Phosphonium salts containing at least one heteroatomic substituent with LPE are classified as quasi-phosphonium compounds with a very high reactivity [66]. Among them, quasi-phosphonium salts with dialkylamine substituents have the greatest stability. It should also be noted that dialkylamine substituents are more hydrophilic and the corresponding amino-quasi-phosphonium salts with a methyl group at the phosphorus atom are even soluble in water [67]. Indeed, it was shown in [68–70] that the amine substituent contributes to the effective delocalization of the positive charge in phosphonium salts due to the p_π–d_π-conjugation of the nitrogen LPE with the *d*-orbitals of the phosphorus atom (Scheme 1).

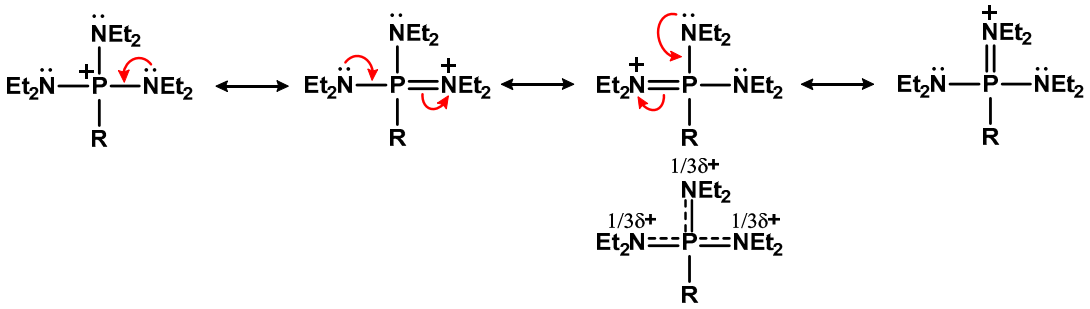

Scheme 1. Delocalization of positive charge in aminophosphonium cations.

Taking into account the above, in this work we synthesized various amphiphilic salts of phosphonium bearing a diethylamine substituent, evaluated their cytotoxicity in vitro and toxicity *in vivo*, and developed nanotherapeutic forms for their delivery.

2. Materials and Methods

2.1. General

The NMR spectra were recorded at 25 °C using a Bruker Avance-400 NMR spectrometer (400.0 MHz, ^{1}H; 100.6 MHz, ^{13}C; 162.0 MHz, ^{31}P), a Bruker Avance-500 NMR spectrometer (500.0 MHz, ^{1}H; 125.8 MHz, ^{13}C; 202.4 MHz, ^{31}P) and a Bruker Avance-600 NMR spectrometer (600.0 MHz, ^{1}H; 150.9 MHz, ^{13}C; 242.94 MHz, ^{31}P). The chemical shifts were measured on the δ scale relative to TMS, using residual protons or carbon signals of $CDCl_3$ or another solvent (^{1}H and ^{13}C) as an internal standard or H_3PO_4 as an external standard. Coupling constant (*J*) values are given in Hz. The ESI MS measurements were performed using an Amazon X ion trap mass spectrometer (Bruker Daltonic GmbH, Germany) in positive mode in the mass range of 70–3000. The capillary voltage was −3500 V, nitrogen drying gas – 10 L·min^{-1}, desolvation temperature – 250 °C. Data processing was performed by Data Analysis 4.0 SP4 software (Bruker Daltonik GmbH, Germany). Melting points were determined on a Melting Point Apparatus Stuart SMP10. Elemental analysis was accomplished with an automated EuroVector EA3000 CHNS-O elemental analyzer (Euro-Vector, Italy). Reactions course was monitored by ^{31}P-{^{1}H} NMR spectra of the reaction mixtures. Solvents were purified and dried by standard protocols. Starting P(III) derivatives were synthesized in accordance with literature data [71] (compound **1**, δ_P 119.0 ppm, MeCN), [72] (compound **2**, δ_P 99.4 ppm, Et_2O), [73] (compound **3**, δ_P 62.9 ppm, CH_2Cl_2). Compound **7** was obtained in acetonitrile according to the data for triethyl(octyl)ammonium bromide [74]. The interpretation of its ^{13}C NMR spectrum was made taking

Preprints (www.preprints.org) | NOT PEER-REVIEWED | Posted: 22 September 2023 doi:10.20944/preprints202309.1553.v1

in account the data of the work [75]. The interpretation of the ^{13}C NMR spectrum of compound **8** was made taking in account the data for octyltriphenylphosphonium bromide [40].

XRD of **6a** performed on a Bruker D8 QUEST automatic three-circle diffractometer at 130 (graphite monochromator, λMoK_α = 0.71073Å, ω- and φ-scan with a step of 0.5°) at the Distributed Spectral-Analytical Center of Shared Facilities for Study of Structure, Composition and Properties of Substances and Materials of FRC Kazan Scientific Center of RAS. Single crystals of a suitable size were glued to the top of a glass fiber in a random orientation. The preliminary unit cell parameters were determined using three runs at different φ angle positions with 12 frames per run (φ-scan technique). The X-ray diffraction data were collected and indexed and the unit cell parameters were determined and refined using the APEX2 software package [76]. The empirical absorption correction based on the crystal shape and an additional spherical correction were applied and systematic errors were corrected using the SADABS software [77]. The structure was solved by direct method using the SHELXT-2014/5 program [78] and refined by the full-matrix least-squares method based on F^2 using the SHELXL-2018/3 program [79] as implemented in WinGX-2020.1 [80]. Non-hydrogen atoms were refined with anisotropic displacement parameters. Hydrogen atoms at carbon atoms were positioned geometrically and refined using a riding model. Intermolecular interactions were analyzed and the figures were generated with the PLATON [81] and Mercury 2020.3 [82] programs, respectively. Crystallographic data for the structures of **6a** were deposited with the Cambridge Crystallographic Data Centre (No *CCDC* 2293515). The X-ray diffraction data collection and structure refinement statistics are given in Table 1.

Table 1. Principal crystallographic parameters of compound **6a** based on X-ray diffraction data.

Parameter	**6a**	**Parameter**	**6a**
Molecular formula	$C_{22}H_{33}NP$, I,	*Ranges of indices*	
Sum Formula	$C_{22}H_{33}INP$	h	$-13 \le h \le 13$
Molecular weight	469.36	k	$-14 \le k \le 14$
Crystal system	triclinic	l	$-20 \le l \le 20$
Space group	P -1 (No. 2)	Number of total reflections	119684
Z	2	Independent reflections	7633
Unit cell parameters		R_{int}	0.069
a / Å	9.3261(5)	Completeness up to θ = 28.0°	0.994
b / Å	9.9546(5)	$T_{max/min}$	0.7456 / 0.5131
c / Å	13.5060(7)	Number of observed reflections (I > 2σ(I))	7098
α	69.106(2)	Number of reflections / of contraints / number of parameters	7633 / 0 / 229
β / deg	71.494(2)	GOOF	1.068
γ	80.251(2)	R [$I > 2\sigma(I)$]	
V / Å^3	1108.61(10)	R_1	0.0213
d_{calc}/g cm^{-3}	1.406	wR_2	0.0553
Absorption coefficient, μ/mm^{-1}	1.521	*R (based on all reflections)*	
F(000)	480	R_1 *and* wR_2	0.0237 and 0.0561
Θ (min, max)/deg	2.2, 32.0	Residual electron density (ϱ_{max} / ϱ_{min}) / e Å^{-3}	1.14 / –0.50

2.2. Chemistry

2.2.1. General Procedure for the Synthesis of Alkyl Diethylaminophoshonium Derivatives 4a-e, 5a-d, 6a-e, 7.

Equmolar amounts of the corresponding P(III)-derivatives **1**, **2** or **3** (4.0 mmol) and alkyl iodide (4.0 mmol) in 5 mL of anhydrous acetonitrile were stirred at the room temperature under a dry argon atmosphere. After the disappearance of the signal of the phosphorus (III) atom in the ^{31}P NMR spectra of in the reaction mixtures the solvent was evaporated under reduced pressure. The residue was washed with dry diethyl ether (5 × 5 mL) (**4a-d**, **5a-d**, **6a-d**) or with hexane (5 × 5 mL) (**4e**, **6e**). Then, the resulting oil dried under reduced pressure (0.01 mmHg) at 40-50°C for 1-2 h. Compound **6a** crystallized upon keeping at room temperature. Its structure was confirmed by the single crystal X-ray diffraction.

Tris(diethylamino)(hexyl)phosphonium iodide 4a, light yellow oil, yield was 1.80 g (98 %). Anal. C, 47.36; H, 9.71; N, 8.92; P, 6.93 %, calcd for $C_{18}H_{43}IN_3P$, C, 47.06; H, 9.43; N, 9.15; P, 6.74 %. ESI-MS, *m/z*: 332.29 $[M - I]^+$; calcd for $C_{18}H_{43}N_3P^+$ 332.32. ^{1}H NMR spectrum (400.0 MHz, $CDCl_3$, δ ppm, *J* Hz): 3.18 dq (NCH_2, 12H, $^3J_{PNCH}$ 10.6, $^3J_{HH}$ 7.1), 2.55 m (C^1H_2, 2H), 1.56 m (C^2H_2, C^3H_2, 4H), 1.32-1,33 m (C^4H_2, C^5H_2, 4H), 1.24 t ($NCCH_3$, 18H, $^3J_{HH}$ 7.1), 0.90 t (C^6H_3, 3H, $^3J_{HH}$ 7.0). ^{13}C-{^{1}H} NMR spectrum (100.6 MHz, $CDCl_3$, δC ppm, *J* Hz): 39.43 d (NCH_2, $^2J_{PNC}$ 3.8), 30.99 s (C^4), 30.27 d (C^2, $^2J_{PCC}$ 18.0), 25.74 d (C^1, $^1J_{PC}$ 104.6), 22.21 d (C^3, $^3J_{PCCC}$ 4.3), 22.03 s (C^5), 13.71 s (C^6), 13.24 d ($NCCH_3$, 3H, $^3J_{PNCC}$ 2.8). ^{31}P-{^{1}H} NMR spectrum (162.0 MHz, $CDCl_3$): δ_P 59.2 ppm.

Tris(diethylamino)(octyl)phosphonium iodide 4b, light yellow oil, yield was 1.87 g (96 %). Anal. C, 49.52; H, 9.81; N, 8.55; P, 6.73 %, calcd for $C_{20}H_{47}IN_3P$, C, 49.28; H, 9.72; N, 8.62; P, 6.35 %. ESI-MS, *m/z*: 360.34 $[M - I]^+$; calcd for $C_{20}H_{47}N_3P^+$ 360.35. ^{1}H NMR spectrum (400.0 MHz, $CDCl_3$, δ ppm, *J* Hz): 3.19 dq (NCH_2, 12H, $^3J_{PNCH}$ 10.5, $^3J_{HH}$ 7.1), 2.57 m (C^1H_2, 2H), 1.56 m (C^2H_2, C^3H_2, 4H), 1.29 m (C^4H_2, C^5H_2, C^6H_2, C^7H_2, 8H), 1.25 t ($NCCH_3$, 18H, $^3J_{HH}$ 7.1), 0.89 t (C^8H_3, 3H, $^3J_{HH}$ 7.1). ^{13}C-{^{1}H} NMR spectrum (100.6 MHz, $CDCl_3$, δC ppm, *J* Hz): 30.70 d (NCH_2, $^2J_{PNC}$ 3.7), 31.64 s (C^6), 30.87 d (C^2, $^2J_{PCC}$ 18.0), 29.13 d (C^4, $^4J_{PCCCC}$ 1.7), 28.90 s (C^5), 26.02 d (C^1, $^1J_{PC}$ 104.5), 22.54 s (C^7), 14.04 s (C^8), 13.50 d ($NCCH_3$, $^3J_{PNCC}$ 2.9). ^{31}P-{^{1}H} NMR spectrum (162.0 MHz, $CDCl_3$): δ_P 58.9 ppm.

Tris(diethylamino)(nonyl)phosphonium iodide 4c, light yellow oil, yield was 1.94 g (97 %). Anal. C, 50.08; H, 9.57; N, 8.54; P, 6.39 %, calcd for $C_{21}H_{49}IN_3P$, C, 50.30; H, 9.78; N, 8.38; P, 6.18 %. ESI-MS, *m/z*: 374.37 $[M - I]^+$; calcd for $C_{21}H_{49}N_3P^+$ 374.37. ^{1}H NMR spectrum (400.0 MHz, $CDCl_3$, δ ppm, *J* Hz): 2.93 m (NCH_2, 12H, $^3J_{PNCH}$ 10.6, $^3J_{HH}$ 7.1), 2.67 m (C^1H_2, 2H), 1.31 m (C^2H_2, C^3H_2, 4H), 0.99-1.03 m (C^4H_2, C^5H_2, C^6H_2, C^7H_2, C^8H_2, 10H, $NCCH_3$, 18H, $^3J_{HH}$ 7.1), 0.63 t (C^9H_3, 3H, $^3J_{HH}$ 7.0). ^{13}C-{^{1}H} NMR spectrum (100.6 MHz, $CDCl_3$, δC ppm, *J* Hz): 39.65 d (NCH_2, $^2J_{PNC}$ 3.3), 31.68 s (C^7), 30.81 d (C^2, $^2J_{PCC}$ 18.0), 29.13 s (C^5, C^6), 22.06 br. s (C^4), 25.96 d (C^1, $^1J_{PC}$ 104.6), 22.71 s (C^8), 14.04 s (C^8), 22.48 d (C^3, $^3J_{PCCC}$ 4.4), 14.0 s (C^9), 13.44 d ($NCCH_3$, $^3J_{PNCC}$ 2.4). ^{31}P-{^{1}H} NMR spectrum (162.0 MHz, $CDCl_3$): δ_P 58.8 ppm.

Decyltris(diethylamino)phosphonium iodide 4d, light yellow oil, yield was 1.96 g (95 %). Anal. C, 50.93; H, 9.67; N, 7.92; P, 6.25 %, calcd for $C_{22}H_{51}IN_3P$, C, 51.25; H, 9.97; N, 8.15; P, 6.01 %. ESI-MS, *m/z*: 388.37 $[M - I]^+$; calcd for $C_{21}H_{49}N_3P^+$ 388.38. ^{1}H NMR spectrum (400.0 MHz, $CDCl_3$, δ ppm, *J* Hz): 3.16 dq (NCH_2, 12H, $^3J_{PNCH}$ 10.6, $^3J_{HH}$ 7.1), 2.52 m (C^1H_2, 2H), 1.52 m (C^2H_2, C^3H_2, 4H), 1.22-1.24 m (C^4H_2, C^5H_2, C^6H_2, C^7H_2, C^8H_2, C^9H_2, 12H), 1.22 t ($NCCH_3$, 18H, $^3J_{HH}$ 7.1), 0.86 t ($C^{10}H_3$, 3H, $^3J_{HH}$ 7.1). ^{13}C-{^{1}H} NMR spectrum (100.6 MHz, $CDCl_3$, δC ppm, *J* Hz): 39.48 d (NCH_2, $^2J_{PNC}$ 3.4), 31.58 s (C^8), 30.67 d (C^2, $^2J_{PCC}$ 17.9), 22.37 d (C^3, $^3J_{PCCC}$ 3.7), 29.22 s (C^5), 29.04 s and 29.00 s (C^6, C^7), 28.97 br. s (C^4), 25.80 d (C^1, $^1J_{PC}$ 104.5), 22.31 s (C^9), 13.90 s (C^{10}), 13.30 d ($NCCH_3$, $^3J_{PNCC}$ 2.3). ^{31}P-{^{1}H} NMR spectrum (162.0 MHz, $CDCl_3$): δ_P 58.7 ppm.

Tris(diethylamino)(tetradecyl)phosphonium bromide 4e, light yellow oil, yield was 1.91 g (91 %). Anal. C, 59.81; H, 11.47; N, 8.29; P, 6.22 %, calcd for $C_{26}H_{59}BrN_3P$, C, 59.52; H, 11.33; N, 8.01; P, 5.90 %. ESI-MS, *m/z*: 444.38 $[M - Br]^+$; calcd for $C_{26}H_{59}N_3P^+$ 444.44. ^{1}H NMR spectrum (400.0 MHz, $CDCl_3$, δ ppm, *J* Hz): 3.15 dq (NCH_2, 12H, $^3J_{PNCH}$ 10.6, $^3J_{HH}$ 7.1), 2.54 m (C^1H_2, 2H), 1.51 m (C^2H_2, C^3H_2, 4H), 1.23 m and 0.85 t (C^4H_2-$C^{13}H_2$, $NCCH_3$, 38H), 0.85 t ($C^{14}H_3$, 3H, $^3J_{HH}$ 7.0). ^{1}H NMR spectrum (500.0 MHz, CD_3CN, δ ppm, *J* Hz): 2.95 dq (NCH_2, 12H, $^3J_{PNCH}$ 10.7, $^3J_{HH}$ 7.0), 2.31 m (C^1H_2, 2H), 1.32 m (C^2H_2,

Preprints (www.preprints.org) | NOT PEER-REVIEWED | Posted: 22 September 2023 doi:10.20944/preprints202309.1553.v1

C^3H_2, 4H), 1.07-1.09 m, 1.03 br.m, 1.02 t (C^4H_2-$C^{13}H_2$, $NCCH_3$, 38H), 0.66 t ($C^{14}H_3$, 3H, $^3J_{HH}$ 7.1). ^{13}C NMR spectrum (125.8 MHz, $CDCl_3$, δ_C ppm, *J* Hz) (here and further, the signal type in the ^{13}C-{^1H} NMR spectrum is shown in parentheses): 39.30 tqd (d) (NCH_2, $^1J_{HC}$ 137.9, $^2J_{PNC}$ 3.5, $^2J_{HCC}$ 4.0), 31.43 tm (s) (C^{12}, $^1J_{HC}$ 130.3,), 30.47 tdm (d) (C^2, $^1J_{HC}$ 124.7, $^2J_{PCC}$ 19.7), 29.18 tm (s) (C^6, $^1J_{HC}$ 125.2), 29.15 tm (s) (C^7 and C^8, $^1J_{HC}$ 125.2), 29.13 tm (s) (C^9, $^1J_{HC}$ 125.2), 29.04 tm (s) (C^{10}, $^1J_{HC}$ 125.0-126.0,), 28.85 tm (br. s) (C^5, C^{11}, $^1J_{HC}$ 127.5-128.0), 28.75 tm (d) (C^4, $^1J_{HC}$ 127.0-128.0, $^4J_{PCCCC}$ 1.5), 25.0 tdm (d) (C^1, $^1J_{HC}$ 128.6, $^1J_{PC}$ 104.4, $^2J_{HCC}$ 4.0, $^3J_{HCCC}$ 2.6), 22.19 tm (s) (C^{13}, $^1J_{HC}$ 128.1), 22.17, tm (d) (C^3, $^1J_{HC}$ 127.0-128.0, $^3J_{PNCC}$ 2.6, $^3J_{PCCC}$ 4.5). ^{31}P-{^1H} NMR spectrum (162.0 MHz, CH_3CN): δ_P 60.4 ppm. ^{31}P-{^1H} NMR spectrum (162.0 MHz, $CDCl_3$): δ_P 59.9 ppm.

Bis(diethylamino)(hexyl)(phenyl)phosphonium iodide 5a, light yellow oil, yield was 1.80 g (97 %). Anal. C, 51.93; H, 7.90; N, 5.89; P, 6.45 %, calcd for $C_{20}H_{38}IN_2P$, C, 51.72; H, 8.25; N, 6.03; P, 6.67 %. ESI-MS, *m/z*: 337.17 [M – I]$^+$; calcd for $C_{20}H_{38}N_2P^+$ 337.28. ^1H NMR spectrum (400.0 MHz, $CDCl_3$, δ ppm, *J* Hz): 7.39-7.42 m (H^o, H^m, H^p, 5H), 2.92 m (NCH_2, 8H, $^3J_{PNCH}$ 10.3, $^3J_{HH}$ 7.1), 2.45 m (C^1H_2, 2H), 1.11 m (C^2H_2, C^3H_2, 4H), 0.87-0.88 two m, 0.87 and 0.88 two t (C^4H_2, C^5H_2, $NCCH_3$, 16H, $^3J_{HH}$ 7.1), 0.46 br. m (C^6H_3, 3H). ^{13}C NMR spectrum (100.6 MHz, $CDCl_3$, δ_C ppm, *J* Hz): 134.45 dtd (d) (C^p, $^1J_{HC}$ 162.6, $^3J_{HCCC}$ 7.0, $^4J_{PCCCC}$ 2.8), 132.11 dddd (d) (C^o, $^1J_{HC}$ 162.9, $^2J_{PCC}$ 10.5, $^3J_{HCCC}$ 6.6-6.8, $^3J_{HCCC}$ 6.6), 129.93 ddd (d) (C^m, $^1J_{HC}$ 165.8, $^3J_{PCCC}$ 13.1, $^3J_{HCCC}$ 6.6), 120.72 dt (d) (C^i, $^1J_{PC}$ 122.9, $^3J_{HCCC}$ 7.3), 40.20 tqd (d) (NCH_2, $^1J_{HC}$ 137.9, $^2J_{HCC}$ 3.7, $^2J_{PNC}$ 2.6), 30.63 tm (s) (C^4, $^1J_{HC}$ 122.0-124.0), 29.58 tdm (d) (C^2, $^1J_{HC}$ 125.0-126.0, $^2J_{PCC}$ 17.1), 24.54 tdm (d) (C^1, $^1J_{HC}$ 129.8, $^1J_{PC}$ 81.9, $^3J_{HCCC}$ 3.6-3.7, $^2J_{HCC}$ 3.6-3.7), 21.81 tm (d) (C^3, $^1J_{HC}$ 126.0-128.0, $^2J_{HCC}$ 3.7-4.0, $^3J_{PCCC}$ 3.4), 21.69 tm (s) (C^5, $^1J_{HC}$ 126.0-127.0), 13.44 qm (s) (C^6, $^1J_{HC}$ 124.0-125.0), 13.38 qdt (d) ($NCCH_3$, $^1J_{HC}$ 126.9, $^3J_{PNCC}$ 3.0, $^2J_{HCC}$ 2.8-3.0). ^{31}P-{^1H} NMR spectrum (162.0 MHz, $CDCl_3$): δ_P 58.9 ppm.

Bis(diethylamino)(octyl)(phenyl)phosphonium iodide 5b, light yellow oil, yield was 1.87 g (95 %). Anal. C, 53.93; H, 8.70; P, 6.55 %, calcd for $C_{22}H_{42}IN_2P$, C, 53.66; H, 8.60; N, 5.69; P, 6.29 %. ESI-MS, *m/z*: 365.28 [M – I]$^+$; calcd for $C_{22}H_{42}N_2P^+$ 365.31. ^{31}P-{^1H} NMR spectrum (162.0 MHz, $CDCl_3$): δ_P 59.4 ppm. ^1H NMR spectrum (400.0 MHz, $CDCl_3$, δ ppm, *J* Hz): 7.54-7.60 m (H^o, H^m, H^p, 5H), 3.10 m (NCH_2, 8H, $^3J_{PNCH}$ 10.5, $^3J_{HH}$ 7.1), 2.63 m (C^1H_2, 2H), 1.20-1.29 m (C^2H_2, C^3H_2, 4H), 1.06-1.01 t and br. m ($NCCH_3$, 12H, $^3J_{HH}$ 7.1, C^4H_2-C^7H_2, 8H), 0.63 t (C^8H_3, 3H, $^3J_{HH}$ 7.0). ^{13}C NMR spectrum (100.6 MHz, $CDCl_3$, δ_C ppm, *J* Hz): 134.44 dtd (d) (C^p, $^1J_{HC}$ 164.2, $^3J_{HCCC}$ 7.0, $^4J_{PCCCC}$ 2.9), 132.15 dddd (d) (C^o, $^1J_{HC}$ 162.7, $^2J_{PCC}$ 10.5, $^3J_{HCCC}$ 7.3, $^3J_{HCCC}$ 7.1), 129.94 ddd (d) (C^m, $^1J_{HC}$ 165.6, $^3J_{PCCC}$ 13.1, $^3J_{HCCC}$ 7.1), 120.88 dt (d) (C^i, $^1J_{PC}$ 122.5, $^3J_{HCCC}$ 6.6), 40.32 tqd (d) (NCH_2, $^1J_{HC}$ 138.0, $^2J_{HCC}$ 4.0, $^2J_{PNC}$ 2.9), 31.07 tm (s) (C^6, $^1J_{HC}$ 126.5), 29.92 tdm (d) (C^2, $^1J_{HC}$ 125.0-126.0, $^2J_{PCC}$ 16.9), 28.47 tm (d) (C^4, $^1J_{HC}$ 122.0, $^1J_{HC}$ 126.0, $^4J_{PCCCC}$ 1.3, $^3J_{HCCC}$ 3.4, $^2J_{HCC}$ 3.4), 28.28 tm (s) (C^5, $^1J_{HC}$ 126.3) 24.69 tdm (d) (C^1, $^1J_{HC}$ 129.8, $^1J_{PC}$ 81.7, $^3J_{HCCC}$ 4.0-4.1, $^2J_{HCC}$ 3.4-3.7,), 21.99 tm (s) (C^7, $^1J_{HC}$ 124.4), 21.92 tm (d) (C^3, $^1J_{HC}$ 126.0-128.0, $^3J_{PCCC}$ 3.6), 13.51 qm (s) (C^8, $^1J_{HC}$ 124.4, 128.0, $^3J_{HCCC}$ 2.8-2.9, $^2J_{HCC}$ 2.8-2.9), 13.41 qdt (d) ($NCCH_3$, $^1J_{HC}$ 127.0, $^3J_{PNCC}$ 3.0, $^2J_{HCC}$ 2.9-3.0).

Bis(diethylamino)(nonyl)(phenyl)phosphonium iodide 5c, light yellow oil, yield was 1.94 g (96 %). C, 54.79; H, 8.90; P, 5.85 %, calcd for $C_{23}H_{44}IN_2P$, C, 54.54; H, 8.70; N, 5.53; P, 6.12 %. ESI-MS, *m/z*: 379.30 [M – I]$^+$; calcd for $C_{23}H_{44}N_2P^+$ 379.32. ^1H NMR spectrum (400.0 MHz, $CDCl_3$, δ ppm, *J* Hz): 7.68-7.78 m (H^o, H^m, H^p, 5H), 3.27 m, (NCH_2, 8H, $^3J_{PNCH}$ 10.5, $^3J_{HH}$ 7.2), 2.84 m (C^1H_2, 2H), 1.37-1.46 m (C^2H_2, C^3H_2, 4H), 1.23 and 1.18 two br. m (C^4H_2-C^8H_2, 10 H), 1.23 t ($NCCH_3$, 12H, $^3J_{HH}$ 7.2), 0.82 t (C^9H_3, 3H, $^3J_{HH}$ 7.1). ^{13}C NMR spectrum (100.6 MHz, $CDCl_3$, δ_C ppm, *J* Hz): 134.33 dtd (d) (C^p, $^1J_{HC}$ 163.7, $^3J_{HCCC}$ 7.3, $^4J_{PCCCC}$ 2.9), 132.07 dddd (d) (C^o, $^1J_{HC}$ 162.8, $^2J_{PCC}$ 10.5, $^3J_{HCCC}$ 7.1, $^3J_{HCCC}$ 6.8), 129.85 ddd (d) (C^m, $^1J_{HC}$ 165.2, $^3J_{PCCC}$ 13.1, $^3J_{HCCC}$ 7.0), 120.78 dt (d) (C^i, $^1J_{PC}$ 122.5, $^3J_{HCCC}$ 7.7), 40.23 tdq (d) (NCH_2, $^1J_{HC}$ 137.8, $^2J_{HCC}$ 4.0, $^2J_{PNC}$ 2.8), 31.10 tm (s) (C^7, $^1J_{HC}$ 126.8), 29.82 tdm (d) (C^3, $^1J_{HC}$ 125.0-126.0, $^3J_{PCCC}$ 16.9), 28.49 tm (br. s) (C^4, $^1J_{HC}$ 122.0-124.0, 28.44 tm (s) (C^5, C^6, $^1J_{HC}$ 124.0-125.0), 24.0 tdm (d) (C^1, $^1J_{HC}$ 130.0, $^1J_{PC}$ 81.7), 21.92 tm (s) (C^8, $^1J_{HC}$ 124.0), 21.87 tm (d) (C^3, $^1J_{HC}$ 126.0-128.0, $^3J_{PCCC}$ 3.3), 13.45 tm (s) (C^9, $^1J_{HC}$ 124.7, $^3J_{HCCC}$ 3.0, $^2J_{HCC}$ 3.0), 13.33 qdt (d) ($NCCH_3$, $^1J_{HC}$ 127.2, $^3J_{PNCC}$ 3.1, $^2J_{HCC}$ 2.8). ^{31}P-{^1H} NMR spectrum (162.0 MHz, $CDCl_3$): δ_P 59.4 ppm.

Decylbis(diethylamino)(phenyl)phosphonium iodide 5d, light yellow oil, yield was 1.98 g (95 %). Anal. C, 55.65; H, 8.99; N, 5.02; P, 6.24 %, calcd for $C_{24}H_{46}IN_2P$, C, 55.38; H, 8.91; N, 5.38; P, 5.95 %. ESI-MS, *m/z*: 393.31 [M – I]$^+$; calcd for $C_{24}H_{46}N_2P^+$ 393.34. ^1H NMR spectrum (400.0 MHz, $CDCl_3$, δ ppm, *J* Hz): 7.59-7.65 m (H^o, H^m, H^p, 5H), 3.15 m, (NCH_2, 8H, $^3J_{PNCH}$ 10.8, $^3J_{HH}$ 7.1), 2.70 m (C^1H_2, 2H), 1.29-1.32 m (C^2H_2, C^3H_2, 4H), 1.11 t ($NCCH_3$, 12H, $^3J_{HH}$ 7.1), 1.11 and 1.06 two m (C^4H_2-C^9H_2, 12H),

Preprints (www.preprints.org) | NOT PEER-REVIEWED | Posted: 22 September 2023 doi:10.20944/preprints202309.1553.v1

0.71 t (C^2H_2 and 1.18 two br. m (C^4H_2-C^8H_2, 10 H), 1.23 t (NCH_3, 12H, $^3J_{HH}$ 7.2), 0.71 t ($C^{10}H_3$, 3H, $^3J_{HH}$ 7.0). ^{13}C NMR spectrum (100.6 MHz, $CDCl_3$, δc ppm, *J* Hz): 134.48 dtd (d) (C^p, $^1J_{HC}$ 163.4, $^3J_{HCCC}$ 6.3, $^4J_{PCCCC}$ 2.9), 132.20 dddd (d) (C^o, $^1J_{HC}$ 162.1, $^2J_{PCC}$ 10.6, $^3J_{HCCC}$ 7.2, $^3J_{HCCC}$ 7.1), 129.98 ddd (d) (C^m, $^1J_{HC}$ 165.4, $^3J_{PCCC}$ 13.1, $^3J_{HCCC}$ 7.0), 120.93 dt (d) (C^i, $^1J_{PC}$ 122.5, $^3J_{HCCC}$ 7.5), 40.37 tqd (d) (NCH_2, $^1J_{HC}$ 127.9, $^2J_{HCC}$ 4.0, $^2J_{PNC}$ 2.9), 31.29 tm (s) (C^8, $^1J_{HC}$ 124.4, $^3J_{HCCC}$ 3.2-3.5, $^2J_{HCC}$ 3.5-4.0), 29.97 tdm (d) (C^2, $^1J_{HC}$ 126.0-127.0, $^2J_{PCC}$ 16.8), 28.89 tm (s) (C^5, $^1J_{HC}$ 126.0-127.0), 28.68 (C^6, C^7, $^1J_{HC}$ 127.0-1280), 28.38 tm (d) (C^4, $^1J_{HC}$ 127.0-128.0, $^4J_{PCCCC}$ 1.2), 24.75 tm (d) (C^1, $^1J_{HC}$ 129.2, $^1J_{PC}$ 81.7), 22.10 tm (s) (C^9, $^1J_{HC}$ 124.4, $^3J_{HCCC}$ 3.7, $^2J_{HCC}$ 3.7), 21.98 tdm (d) (C^3, $^1J_{HC}$ 128.0, $^3J_{PCCC}$ 3.5), 13.60 qm (C^{10}, $^1J_{HC}$ 124.3, $^3J_{HCCC}$ 3.3-3.4, $^2J_{HCC}$ 3.5-4.0), 13.45 qdt ($NCCH_3$, $^1J_{HC}$ 127.1, $^3J_{PNCC}$ 3.0, $^2J_{HCC}$ 3.0). ^{31}P-{^{1}H} NMR spectrum (162.0 MHz, $CDCl_3$): δ_P 59.2 ppm.

(Diethylamino)(hexyl)diphenylphosphonium iodide 6a, colorless crystals, yield was 1.84 g (98 %), mp 91-93°C. Anal. C, 56.55; H, 6.89; N, 3.21; P, 6.44 %, calcd for $C_{22}H_{33}INP$, C, 56.29; H, 7.09; N, 2.98; P, 6.60 %. ESI-MS, *m*/*z*: 342.13 [M – I]$^+$; calcd for $C_{22}H_{33}NP^+$ 342.24. ^{1}H NMR spectrum (400.0 MHz, $CDCl_3$, δ ppm, *J* Hz): 7.85 m and 7.81 m (H^o, H^p, 6H, $^3J_{PCCH^o}$ 12.4, $^3J_{H^oH^m}$ 7.7, $^3J_{H^mH^p}$ 7.7, $^5J_{PCCCCH^p}$ 1.5, $^4J_{H^mCCCH^p}$ 1.4), 7.73 m (H^m, 4H, $^3J_{H^pH^m}$ 7.7, $^3J_{H^oH^m}$ 7.7, $^4J_{PCCCH^m}$ 3.5), 3.31 dq and 3.30 m (NCH_2, C^1H_2, 6H), 1.50-1.54 m (C^2H_2, C^3H_2, 4H), 1.21-1.23 m (C^4H_2, C^5H_2, 4H), 1.14 t ($NCCH_3$, 6H), 0.81 br. t (C^6H_3, 3H, $^3J_{HH}$ 7.1). ^{13}C NMR spectrum (100.6 MHz, $CDCl_3$, δc ppm, *J* Hz): 134.33 dtd (d) (C^p, $^1J_{HC}$ 163.3, $^3J_{HCCC}$ 7.4, $^4J_{PCCCC}$ 2.6), 132.14 dddd (d) (C^o, $^1J_{HC}$ 163.5, $^3J_{HCCC}$ 7.4, $^2J_{PCC}$ 10.4), 129.61 ddd (d) (C^m, $^1J_{HC}$ 165.6, $^3J_{PCCC}$ 12.6, $^3J_{HCCC}$ 7.3), 119.40 dt (d) (C^i, $^1J_{PC}$ 96.4, $^3J_{HCCC}$ 7.4), 40.95 tqd (d) (NCH_2, $^1J_{HC}$ 138.3, $^2J_{HCC}$ 4.1, $^2J_{PNC}$ 2.3), 30.24 tm (s) (C^4, $^1J_{HC}$ 124.7), 29.22 tdm (d) (C^2, $^1J_{HC}$ 127.0-128.0, $^2J_{PCC}$ 16.0), 23.71 tdm (d) (C^1, $^1J_{HC}$ 130.6, $^1J_{PC}$ 63.1, $^3J_{HCCC}$ 3.0-4.0, $^2J_{HCC}$ 3.0-4.0), 21.47 tm (d) (C^3, $^1J_{HC}$ 124.3, $^2J_{HCC}$ 3.7-4.0, $^3J_{HCCC}$ 3.7-4.0, $^3J_{PCCC}$ 3.5), 21.31 tm (s) (C^5, $^1J_{HC}$ 125.3), 13.12 qdt (d) ($NCCH_3$, $^1J_{HC}$ 127.1, $^3J_{PNCC}$ 2.4, $^2J_{HCC}$ 2.7), 13.08 qm (s) (C^6, $^1J_{HC}$ 124.5, $^3J_{HCCC}$ 3.7-4.0, $^2J_{HCC}$ 3.7-4.0). ^{31}P-{^{1}H} NMR spectrum (162.0 MHz, $CDCl_3$): δ_P 52.0 ppm.

(Diethylamino)(octyl)diphenylphosphonium iodide 6b, light yellow oil, yield was 1.91 g (96 %). Anal. C, 58.35; H, 7.19; N, 3.03; P, 6.44 %, calcd for $C_{24}H_{37}INP$, C, 57.95; H, 7.50; N, 2.82; P, 6.24 %. ESI-MS, *m*/*z*: 370.22 [M – I]$^+$. calcd for $C_{24}H_{37}NP^+$ 370.27. ^{1}H NMR spectrum (400.0 MHz, $CDCl_3$, δ ppm, *J* Hz): 7.78-7.83 m and 7.79 m (H^o, H^p, 6H, $^3J_{PCCH^o}$ 12.4, $^3J_{H^oH^m}$ 7.7, $^3J_{H^mH^p}$ 7.7, $^5J_{PCCCCH^p}$ 1.5, $^4J_{H^mCCCH^p}$ 1.4), 7.70 m (H^m, 4H, $^3J_{H^pH^m}$ 7.7, $^3J_{H^oH^m}$ 7.7, $^4J_{PCCCH^m}$ 3.5), 3.27 dk and 3.23 m (NCH_2, C^1H_2, 6H, $^3J_{PNCH}$ 11.3, $^3J_{HH}$ 7.1), 1.45-1.48 m (C^2H_2, C^3H_2, 4H), 1.14-1.18 m and 1.10 t (C^4H_2, C^5H_2, C^6H_2, C^7H_2, $NCCH_3$, 14H, $^3J_{HH}$ 7.1), 0.77 t (C^8H_3, 3H, $^3J_{HH}$ 7.1). ^{13}C NMR spectrum (100.6 MHz, $CDCl_3$, δc ppm, *J* Hz): 134.68 dtd (d) (C^p, $^1J_{HC}$ 163.3, $^3J_{HCCC}$ 7.1, $^4J_{PCCCC}$ 2.8), 132.48 dddd (d) (C^o, $^1J_{HC}$ 163.6, $^3J_{HCCC}$ 7.0, $^2J_{PCC}$ 10.4), 129.96 ddd (d) (C^m, $^1J_{HC}$ 165.8, $^3J_{PCCC}$ 12.6, $^3J_{HCCC}$ 7.4), 119.77 dt (d) (C^i, $^1J_{PC}$ 96.4, $^3J_{HCCC}$ 7.2), 41.31 tdq (d) (NCH_2, $^1J_{HC}$ 138.5, $^2J_{HCC}$ 4.2, $^2J_{PNC}$ 2.3), 31.07 tm (s) (C^6, $^1J_{HC}$ 126.5), 29.92 tdm (d) (C^2, $^1J_{HC}$ 125.0-126.0, $^2J_{PCC}$ 16.0), 28.46 tm (br. s) (C^4, $^1J_{HC}$ 124.0-126.0), 28.25 tm (s) (C^6, $^1J_{HC}$ 126.4), 24.09 tdm (d) (C^1, $^1J_{HC}$ 131.2, $^1J_{PC}$ 63.0, $^3J_{HCCC}$ 3.0-4.0, $^2J_{HCC}$ 3.0-4.0), 21.98 tm (s) (C^7, $^1J_{HC}$ 124.5), 21.87 tm (d) (C^3, $^1J_{HC}$ 126.0-128.0, $^3J_{PCCC}$ 3.5), 13.51 qm (s) (C^8, $^1J_{HC}$ 124.4, $^3J_{HCCC}$ 3.1-3.6, $^2J_{HCC}$ 3.1-3.6), 13.44 qdt (d) ($NCCH_3$, $^1J_{HC}$ 127.3, $^3J_{PNCC}$ 2.6, $^2J_{HCC}$ 2.8). ^{31}P-{^{1}H} NMR spectrum (162.0 MHz, $CDCl_3$): δ_P 51.9 ppm.

(Diethylamino)(nonyl)diphenylphosphonium iodide 6c, light yellow oil, yield was 1.94 g (95 %). Anal. C, 58.45; H, 7.89; N, 2.96; P, 5.84 %, calcd for $C_{25}H_{39}INP$, C, 58.71; H, 7.69; N, 2.74; P, 6.07 %. ESI-MS, *m*/*z*: 384.18 [M – I]$^+$; calcd for $C_{25}H_{39}NP^+$ 384.28. ^{31}P-{^{1}H} NMR spectrum (162.0 MHz, CH_3CN): δ_P 52.2 ppm. ^{1}H NMR spectrum (400.0 MHz, $CDCl_3$, δ ppm, *J* Hz): 7.70 m and 7.68 m (H^o, H^p, 6H, $^3J_{PCCH^o}$ 12.4, $^3J_{H^oH^m}$ 7.7, $^3J_{H^mH^p}$ 7.7, $^5J_{PCCCCH^p}$ 1.5, $^4J_{H^mCCCH^p}$ 1.4), 7.60 m (H^m, 4H, $^3J_{H^pH^m}$ 7.7, $^3J_{H^oH^m}$ 7.7, $^4J_{PCCCH^m}$ 3.5), 3.16 dq (NCH_2, 4H, $^3J_{PNCH}$ 11.3, $^3J_{HH}$ 7.1), 3.10 m (C^1H_2, 2H), 1.35-1.38 m (C^2H_2, C^3H_2, 4H), 1.05-1.08 m and 1.04 br. m (C^4H_2, C^5H_2, C^6H_2, C^7H_2, C^8H_2, 10H), 1.0 t ($NCCH_3$, 6H, $^3J_{HH}$ 7.1), 0.67 t (C^9H_3, 3H, $^3J_{HH}$ 7.1).^{13}C NMR spectrum (100.6 MHz, $CDCl_3$, δc ppm, *J* Hz): 134.79 dtd (d) (C^p, $^1J_{HC}$ 164.2, $^3J_{HCCC}$ 7.1, $^4J_{PCCCC}$ 2.9), 132.59 dddd (d) (C^o, $^1J_{HC}$ 163.6, $^3J_{HCCC}$ 7.4, $^2J_{PCC}$ 10.6), 130.07 ddd (d) (C^m, $^1J_{HC}$ 165.8, $^3J_{PCCC}$ 12.6, $^3J_{HCCC}$ 7.3), 119.88 dt (d) (C^i, $^1J_{PC}$ 96.4, $^3J_{HCCC}$ 8.4), 41.42 tqd (d) (NCH_2, $^1J_{HC}$ 138.4, $^2J_{HCC}$ 4.0, $^2J_{PNC}$ 3.0), 31.31 tm (s) (C^7, $^1J_{HC}$ 125.0-126.0), 30.04 tdm (d) (C^2, $^1J_{HC}$ 125.0-126.0, $^2J_{PCC}$ 16.0), 28.68 and 28.66 two tm (two s) (C^5, C^6, $^1J_{HC}$ 124.0-125.0), 28.64 tm (br. s) (C^4, $^1J_{HC}$ 122.0-124.0), 24.23 tdm (d) (C^1, $^1J_{HC}$ 131.1, $^1J_{PC}$ 63.0), 22.14 tm (s) (C^8, $^1J_{HC}$ 124.2), 21.99 tm (d) (C^3, $^1J_{HC}$ 126.0-128.0, $^3J_{PCCC}$ 3.7), 13.66 qm (s) (C^9, $^1J_{HC}$ 124.5, $^3J_{HCCC}$ 3.5-4.0, $^2J_{HCC}$ 3.5-4.0), 13.55 qdt (d) ($NCCH_3$, $^1J_{HC}$ 127.3, $^3J_{PNCC}$ 2.6, $^2J_{HCC}$ 2.7). ^{31}P-{^{1}H} NMR spectrum (162.0 MHz, $CDCl_3$): δ_P 52.0 ppm.

Preprints (www.preprints.org) | NOT PEER-REVIEWED | Posted: 22 September 2023 doi:10.20944/preprints202309.1553.v1

Decyl(diethylamino)diphenylphosphonium iodide 6d, light yellow oil, yield was 1.97 g (94 %). Anal. C, 59.65; H, 8.18; N, 2.83; P, 6.14 %, calcd for $C_{26}H_{41}INP$, C, 59.43; H, 7.86; N, 2.67; P, 5.90 %. ESI-MS, *m*/*z*: 398.27 $[M - I]^+$; calcd for $C_{26}H_{41}NP^+$ 398.30. ^{1}H NMR spectrum (400.0 MHz, $CDCl_3$, δ ppm, *J* Hz): 7.79 m and 7.76 m (H^o, H^p, 6H, $^3J_{PCCH^o}$ 12.4, $^3J_{H^oH^m}$ 7.7, $^3J_{H^mH^p}$ 7.7, $^5J_{PCCCH^p}$ 1.4, $^4J_{H^mCCCH^p}$ 1.3), 7.68 m (H^m, 4H, $^3J_{H^pH^m}$ 7.7, $^3J_{H^oH^m}$ 7.7, $^4J_{PCCCH^m}$ 3.5), 3.25 dq (NCH_2, 4H, $^3J_{PNCH}$ 11.3, $^3J_{HH}$ 7.1), 3.20 m (C^1H_2, 2H), 1.44-1.48 m (C^2H_2, C^3H_2, 4H), 1.15-1.17 m and 1.12 br. m (C^4H_2, C^5H_2, C^6H_2, C^7H_2, C^8H_2, C^9H_2, 12H), 1.08 t ($NCCH_3$, 6H, $^3J_{HH}$ 7.1), 0.77 t ($C^{10}H_3$, 3H, $^3J_{HH}$ 7.1). ^{13}C NMR spectrum (100.6 MHz, $CDCl_3$, δ_C ppm, *J* Hz): 135.07 dtd (d) (C^p, $^1J_{HC}$ 163.3, $^3J_{HCCC}$ 7.3, $^4J_{PCCCC}$ 2.9), 132.90 dddd (d) (C^o, $^1J_{HC}$ 163.5, $^3J_{HCCC}$ 7.1, $^2J_{PCC}$ 10.5), 130.34 ddd (d) (C^m, $^1J_{HC}$ 165.8, $^3J_{PCCC}$ 12.6, $^3J_{HCCC}$ 7.4), 120.33 dt (d) (C^i, $^1J_{PC}$ 96.6, $^3J_{HCCC}$ 7.4), 41.73 tqd (d) (NCH_2, $^1J_{HC}$ 139.5, $^2J_{HCC}$ 4.2, $^2J_{PNC}$ 2.7), 31.67 tm (s) (C^8, $^1J_{HC}$ 126.0-127.0), 30.36 tdm (d) (C^2, $^1J_{HC}$ 125.0-126.0, $^2J_{PCC}$ 16.0), 29.28 tm (s) (C^7, $^1J_{HC}$ 127.1), 29.07 and 29.04 two tm (two s) (C^5, C^6, $^1J_{HC}$ 124.0-125.0), 28.97 tm (br. s) (C^4, $^1J_{HC}$ 122.0-124.0), 24.55 tdm (d) (C^1, $^1J_{HC}$ 132.1, $^1J_{PC}$ 62.9), 22.48 tm (s) (C^9, $^1J_{HC}$ 124.0-125.0), 22.31 tm (d) (C^3, $^1J_{HC}$ 126.0-128.0, $^3J_{PCCC}$ 3.5), 13.96 qm (s) (C^{10}, $^1J_{HC}$ 125.1), 13.82 qdt (d) ($NCCH_3$, $^1J_{HC}$ 127.4, $^3J_{PNCC}$ 2.6, $^2J_{HCC}$ 2.8). ^{31}P-{^{1}H} NMR spectrum (162.0 MHz, $CDCl_3$): δ_P 51.1 ppm.

(Diethylamino)diphenyl(tetradecyl)phosphonium bromide 6e, light yellow oil, yield was 1.99 g (93 %). Anal. C, 67.19; H, 8.89; N, 2.73; P, 6.14 %, calcd for $C_{30}H_{49}BrNP$, C, 67.40; H, 9.24; N, 2.62; P, 5.80 %. ESI-MS, *m*/*z*: 454.35 $[M - Br]^+$; calcd for $C_{30}H_{49}NP^+$ 454.36. ^{1}H NMR spectrum (400.0 MHz, $CDCl_3$, δ ppm, *J* Hz): 7.85 m (H^o, 4H, $^3J_{PCCH^o}$ 12.3-13.4, $^3J_{H^oH^m}$ 7.7, $^4J_{H^oH^p}$ 1.4), 7.79 m (H^p, 2H, $^3J_{H^pH^m}$ 7.7, $^4J_{H^pH^o}$ 1.4, $^5J_{PH^p}$ 1.6), 7.70 m (H^m, 4H, $^3J_{H^mH^o}$ 7.7, $^3J_{HH}$ 7.7, $^4J_{PH}$ 3.5), 3.37 m (C^1H_2, 2H), 3.30 dq (d) (NCH_2, 4H, $^3J_{PNCH}$ 11.3, $^3J_{HH}$ 7.1), 1.48-1.49 m (C^2H_2, C^3H_2, 4H), 1.21 and 1.16 two br. m (C^4H_2-$C^{13}H_2$, 20H), 1.12 t ($NCCH_3$, 6H, $^3J_{HH}$ 7.1), 0.84 t ($C^{14}H_3$, 3H, $^3J_{HH}$ 7.1). ^{1}H NMR spectrum (500.0 MHz, $CDCl_3$, δ ppm, *J* Hz): 7.54 m (H^o, 4H, $^3J_{PH^o}$ 12.4, $^3J_{H^oH^m}$ 7.7), 7.47 m (H^p, 2H, $^3J_{H^pH^m}$ 7.1), 7.40 m (H^m, 4H, $^3J_{H^mH^o}$ 7.7, $^3J_{HH}$ 7.7, $^4J_{PH}$ 3.5), 2.97-3.00 m (NCH_2, C^1H_2, 6H, $^3J_{PNCH}$ 11.3, $^3J_{HH}$ 7.1), 1.16-1.17 m (C^2H_2, C^3H_2, 4H), 0.86-0.88 m, 0.83 br. m, 0.79 t (C^4H_2-$C^{13}H_2$, $NCCH_3$, 26H, $^3J_{HH}$ 7.1), 0.48 t ($C^{14}H_3$, 3H, $^3J_{HH}$ 7.1). ^{13}C NMR spectrum (125.8 MHz, $CDCl_3$, δ_C ppm, *J* Hz): 134.24 dtd (d) (C^p, $^1J_{HC}$ 163.7, $^3J_{HCCC}$ 7.5, $^4J_{PCCCC}$ 2.5), 132.12 dddd (d) (C^o, $^1J_{HC}$ 164.1, $^2J_{PCC}$ 10.4, $^3J_{HCCC}$ 7.2, $^3J_{HCCC}$ 6.9), 129.53 ddd (d) (C^m, $^1J_{HC}$ 166.0, $^3J_{PCCC}$ 12.6, $^3J_{HCCC}$ 7.4), 119.54 dt (d) (C^i, $^1J_{PC}$ 96.3, $^3J_{HCCC}$ 8.2), 40.78 tqd (d) (NCH_2, $^1J_{HC}$ 139.3, $^2J_{HCC}$ 4.0, $^2J_{PNC}$ 1.9), 30.95 tm (s) (C^{12}, $^1J_{HC}$ 126.0), 29.55 tdm (d) (C^2, $^1J_{HC}$ 124.0-125.0, $^2J_{PCC}$ 16.0), 28.70 tm (s) (C^6, $^1J_{HC}$ 124.0-125.0), 28.67 tm (s) (C^7, C^8, $^1J_{HC}$ 124.0-125.0), 28.63 tm (br. s) (C^4, $^1J_{HC}$ 124.0-125.0), 28.54 tm (s) (C^{10}, $^1J_{HC}$ 124.0-125.0), 28.37 tm (s) (C^{11}, $^1J_{HC}$ 124.0-125.0), 28.26 tm (s) (C^5, $^1J_{HC}$ 124.0-125.0), 28.17 tm (br. s) (C^4, $^1J_{HC}$ 124.0-125.0), 23.42 tdm (d) (C^1, $^1J_{HC}$ 130.9, $^1J_{PC}$ 62.8, $^3J_{HCCC}$ 3.0-4.0), 21.72 tm (s) (C^{13}, $^1J_{HC}$ 126.5), 21.52 tm (d) (C^3, $^1J_{HC}$ 128-129.0, $^3J_{PCCC}$ 3.4), 13.22 qm (s) (C^{14}, $^1J_{HC}$ 124.5, $^3J_{HCCC}$ 3.3-4.0), 12.97 qdt (d) ($NCCH_3$, $^1J_{HC}$ 127.3, $^2J_{HCC}$ 2.7, $^3J_{PNCC}$ 2.2). ^{31}P-{^{1}H} NMR spectrum (162.0 MHz, $CDCl_3$): δ_P 52.0 ppm. ^{31}P-{^{1}H} NMR spectrum (162.0 MHz, CH_3CN): δ_P 51.9 ppm.

Triethyloctylammonium iodide 7. The mixture of triethylamine (3 g, 29.7 mmol) and octyl iodide (6.42 g, 26.8 mmol) in 5 ml of dry acetonitrile was refluxed for 1 h. Acetonitrile was removed in vacuo, the remaining powder was washed with diethyl ether (3 × 4 mL) and was dried in vacuo. Yield was 8.66 g (95%), mp 122-123°C. (Lit. 94-97°C [83]). Anal. C, 49.58; H, 9.55; N, 4.39 %, calcd for $C_{14}H_{32}IN$, C, 49.27; H, 9.45, N, 4.10 %. ESI-MS, *m*/*z*: 214.22 $[M - I]^+$; calcd for $C_{14}H_{32}N^+$ 214.25. ^{1}H NMR spectrum (400.0 MHz, $CDCl_3$, δ ppm, *J* Hz): 3.47 q (NCH_2, 6H, $^3J_{HH}$ 7.3), 3.26 m (C^1H_2, 2H), 1.68 m (C^2H_2, 2H), 1.34-1.36 m and 1.38 t (C^3H_2, C^4H_2, $NCCH_3$, 13H), 1.25-1.27 (C^5H_2, C^6H_2, C^7H_2, 6H), 0.87 t (C^8H_3, 3H, $^3J_{HH}$ 7.1). ^{13}C NMR spectrum (100.6 MHz, $CDCl_3$, δ_C ppm, *J* Hz): 56.74 br. t (s) (C^1, $^1J_{HC}$ 142.0), 52.81 br. t (s) (NCH_2, $^1J_{HC}$ 133.5), 30.54 tm (s) (C^6, $^1J_{HC}$ 125.2), 28.66 tm (s) (C^4, $^1J_{HC}$ 128.3), 28.61 tm (s) (C^5, $^1J_{HC}$ 128.3), 25.38 (C^3, $^1J_{HC}$ 125.1), 21.49 (C^2, $^1J_{HC}$ 124.7), 21.17 (C^7, $^1J_{HC}$ 127.6), 13.07 (C^8, $^1J_{HC}$ 124.6), 7.43 ($NCCH_3$, $^1J_{HC}$ 128.7, $^2J_{HCC}$ 3.5).

Octyltriphenylphosphonium iodide 8. The mixture of triphenylphosphine (1.09 g, 4.16 mmol) and octyl iodide (1 g, 4.17 mmol) in 5 mL of dry acetonitrile was refluxed for 1 h. Acetonitrile was removed under reduced pressure, and the obtained oil was washed with diethyl ether (4 × 5 mL) and was dried in vacuo. Yield was 2 g (96 %). Anal. C, 61.89; H, 6.03; P, 5.89 %, calcd for $C_{26}H_{32}IP$, C, 62.16; H, 6.42; P, 6.17 %. ESI-MS, *m*/*z* : 375.25 $[M - I]^+$; calcd for $C_{26}H_{32}P^+$ 375.22. ^{1}H NMR spectrum (400.0

MHz, $CDCl_3$, δ ppm, *J* Hz): 7.76-7.78 m (H^o, H^p, 9H), 7.69 m (H^m, 6H, $^3J_{HH}$ 7.4, $^3J_{HH}$ 7.4, $^4J_{PCCCH}$ 3.5), 3.55 br. m (PCH_2, 2H), 1.59 m (C^2H_2, C^3H_2, 4H), 1.16-1.21 m (C^4H_2-C^7H_2, 8H), 0.79 t (C^8H_3, 3H, $^3J_{HH}$ 7.0). ^{13}C NMR spectrum (here and further, the signal type in the ^{13}C-{^1H} NMR spectrum is shown in parentheses) (125.8 MHz, $CDCl_3$, δ ppm, *J* Hz): 134.71 dtd (d) (C^p, $^1J_{HC}$ 163.8, $^3J_{HCCC}$ 7.4, $^4J_{PCCCC}$ 2.4), 133.07 dddd (d) (C^o, $^1J_{HC}$ 163.5, $^2J_{PCC}$ 9.8, $^3J_{HCCC}$ 7.7, $^3J_{HCCC}$ 7.6), 130.13 ddd (d) (C^m, $^1J_{HC}$ 166.1, $^3J_{PCCC}$ 12.3, $^3J_{HCCC}$ 7.2), 117.45 dt (d) (C^i, $^1J_{PC}$ 85.8, $^3J_{HCCC}$ 8.8), 31.05 tm (s) (C^6, $^1J_{HC}$ 128.2), 29.88 tdm (d) (C^2, $^1J_{HC}$ 128.0-129.0, $^2J_{PCC}$ 15.7), 28.45 tm (br. s) (C^4, $^1J_{HC}$ 124.7), 28.43 tm (s) (C^5, $^1J_{HC}$ 124.0-125.0), 22.60 tdm (d) (C^1, $^1J_{HC}$ 131.1, $^1J_{PC}$ 49.3), 21.95 tm (s) (C^7, $^1J_{HC}$ 124.0-125.0), 21.96 tm (d) (C^3, $^1J_{HC}$ 124.0-125.0, $^2J_{PCC}$ 4.0-5.0), 13.50 qm (s) (C^8, $^1J_{HC}$ 124.1). ^{31}P-{^1H} NMR spectrum (162.0 MHz, $CDCl_3$): δ_P 24.9 ppm.

1,6-Hexanediyl-bis(hexaethyltriaminophosphonium)dibromide 9. The mixture of hexaethyltriaminophosphine (1.98 g, 8 mmol) and 1,6-dibromohexane (0.98 g, 4 mmol) in 7 mL of anhydrous acetonitrile was stirred for 10 h. Acetonitrile was removed under reduced pressure, and the obtained oil was washed with diethyl ether (4 × 5 mL) and was dried in vacuo. Light yellow oil, yield was 2.83 g (96 %). Anal. C, 49.03; H, 9.55; N, 11.02; P, 8.79 %, calcd for $C_{30}H_{72}Br_2N_6P_2$, C, 48.78; H, 9.82; N, 11.38; P, 8.40 %. ESI-MS, *m/z*: 289.12 $[M - 2Br]^{2+}$; calcd for $C_{30}H_{72}N_6P^{2+}$ 289.26. ^1H NMR spectrum (400.0 MHz, $CDCl_3$, δ ppm, *J* Hz): 2.66 br. m (NCH_2, 24H, $^3J_{PNCH}$ 8.1, $^3J_{HH}$ 6.5), 2.46 br. m (C^1H_B, 2H), 2.18 br. m (C^1H_A, 2H), 1.15-1,16 m (C^2H_2, 4H), 0.88 m (C^3H_2, 4H), 0.73 br. t ($NCCH_3$, 36H). ^{13}C NMR spectrum (100.6 MHz, $CDCl_3$, δ_C ppm, *J* Hz): 38.42 tdq (d) (NCH_2, $^1J_{HC}$ 138.0, $^2J_{PNC}$ 3.8, $^2J_{HCC}$ 4.0), 28.62 tdm (d) (C^2, $^1J_{HC}$ 128.5, $^2J_{PCC}$ 18.7), 24.32 tdm (d) (C^1, $^1J_{HC}$ 129.6, $^1J_{PC}$ 104.1, $^3J_{HCCC}$ 2.0, $^2J_{HCC}$ 1.8-2.0,), 21.15 tm (d) (C^3, $^1J_{HC}$ 134.4, $^3J_{PCCC}$ 4.0), 12.29 qdt (d) ($NCCH_3$, $^1J_{HC}$ 127.0, $^3J_{PNCC}$ 2.6, $^2J_{HCC}$ 2.7). ^{31}P-{^1H} NMR spectrum (162.0 MHz, $CDCl_3$): δ_P 60.3 ppm.

2.2. Preparation and Characterization of Lipid Nanoparticles

2.2.1. Chemicals

L-α-phosphatidylcholine (PC) (Soy, 95%, Avanti polar lipids), Precirol® ATO 5 (glyceryl palmitostearate) was a gift from Gattefossé (St-Priest France), Kolliphor P 188 (Lutrol® F68, Poloxamer 188) (oxyethylene, 79.9-83.7%, Sigma-Aldrich, St. Luis, USA), Rhodamine B (99%, ACROS Organics, New Jersey, USA), Curcumine (Sigma-Aldrich, China), Ultra-purified water (18.2 MΩcm resistivity at 25 °C) was produced from Direct-Q 5 UV equipment (Millipore S.A.S. 67120 Molsheim-France). All reagents were used with-out further treatment.

2.2.2. Preparation of Liposomes Modified by Aminophosphonium Salts

L-α-phosphatidylcholine (PC) (5% w/w) and compounds **4**, **5**, **7** and **8** were dissolved in 1 mL of ethanol. The homogeneous solution was kept in a water bath at 60 °C until complete alcohol evaporation to obtain a thin lipid film. Ultra-purified water was pre-heated to 60 °C and added to rehydrate the lipids at 60 °C in the absence. The solution was stirred under magnetic stirring (750 rpm) (Ika, Germany) for 30 min at the same temperature. Then, the solution was kept for 1.5 h in a water bath at 37 °C. The multilamellar liposome systems were extruded 15 times by passage throuh a polycarbonate membrane of 100 nm pore size (Mini-Extruder Extrusion Technique, Avanti Polar Lipids, Inc.). The same method was used for rhodamine B (0.05% w/w)-labeled liposomes.

2.2.3. Preparation of SLN Modified by Aminophosphonium Salts

Briefly, Precirol® ATO 5 (1.5% w/w) was melted at 70°C and compound 5 (0.01% w/w) was added to the melted lipid and dissolved. A pre-emulsion was formed after dispersing the hot lipid phase in a Poloxamer 188 surfactant solution (1% w/w) using Ultra-Turrax® (IKA, T18, Germany) at 8000 rpm for 5 min. The obtained pre-emulsion was passed through a high-pressure homogenizer (Avestin Emulsiflex C5, Canada) at 70°C, applying a pressure of 1200 bar during 15min. The obtained aqueous dispersions were filled in glass vials, which were immediately sealed and stored at room temperature (20°C). Total volume is 50 mL. The same method was used for curcumine-labeled SLN and TPP-SLN by adding 50µL curcumin (C = 0.01M) in methanol to the melted lipid and kept until evaporation of methanol and dissolving of curcumine.

Preprints (www.preprints.org) | NOT PEER-REVIEWED | Posted: 22 September 2023 doi:10.20944/preprints202309.1553.v1

2.2.4. Characterization by DLS

The mean particle size, zeta potential, and polydispersity index were determined by dynamic light scattering (DLS), using a Malvern Instrument Zetasizer Nano (Malvern, Worcestershire, UK). The size (hydrodynamic diameter, nm) was calculated according to the Einstein–Stokes relationship $D = k_B T/3\pi\eta x$, where D is the diffusion coefficient, k_B is the Boltzmann's constant, T is the absolute temperature, η is the viscosity, and x is the hydrodynamic diameter of nanoparticles. The diffusion coefficient was determined at least in triplicate for each sample. The average error of measurements was approximately 10%. All lipid samples were diluted with ultra-purified water to a suitable concentration (2.5 mg/mL) and analyzed in triplicate.

2.2.5. In Vitro Rhodamine B Release Profile

The monitoring of rhodamine B release from liposomes was performed using the dialysis bag diffusion method. Dialysis bags retain liposomes and allow the released rhodamine B to diffuse into the medium. The bags were soaked in Milli-Q water for 12 h before use. Then, 0.5 mL of liposomes was poured into the dialysis bag. The two bag ends were sealed with clamps. The bags were then placed in a vessel containing 100 mL of 0.025 M sodium phosphate buffer pH 7.4, the receiving phase. The vessel was placed in a thermostatic shaker at 37 °C, under a stirring rate of 150 rpm. At predetermined time intervals, 0.5 mL of samples were withdrawn, and their absorbance at 554 nm was measured using Perkin Elmer λ35 (PerkinElmer Instruments, Norwalk, USA). All samples were analyzed in triplicate. The extinction coefficient of rhodamine B is 106,089 M^{-1} cm^{-1} at pH = 7.4.

2.3. Biological Study

Cells and Materials

For experiments, we used tumor cell cultures M-HeLa clone 11, a human epithelioid carcinoma of the cervix (subline HeLa., clone M-HeLa), T 98G, a human glioblastoma; Hep G2, a human liver carcinoma; PANC-1, a human pancreatic carcinoma; HuTu 80, a human duodenal adenocarcinoma; MCF7, a human breast adenocarcinoma (pleural fluid); A549, a human lung carcinoma; WI38, VA 13 subline 2RA, a human embryonic lung from the collection of the Institute of Cytology, Russian Academy of Sciences (St. Petersburg); PC3, a human prostate adenocarcinoma cell line from ATCC (American Type Cell Collection, USA; CRL 1435); human liver cells (Chang liver) from the collection Research Institute of Virology of the Russian Academy of Medical Sciences (Moscow); SK-OV-3, a human ovarian adenocarcinoma; DU-145, a human prostate carcinoma from the CLS Cell Lines Service cell repository.

2.3.1. Cell Toxicity Assay (MTT-Test)

The cytotoxic effect on cells was determined using the colorimetric method of cell proliferation – the MTT test. Cells were seeded on a 96-well Nunc plate at a concentration of 5×10^3 cells per well in a volume of 100 μL of medium and cultured in a CO_2 incubator at 37 °C until a monolayer was formed. Then the nutrient medium was removed and 100 μL of solutions of the test drug in given dilutions were added to the wells, which were prepared directly in the nutrient medium with the addition of DMSO (5% v/v) to improve solubility. After 48 h incubation of cells with the tested compounds, the nutrient medium was removed from the plates, and 100 μL of the nutrient medium without serum containing MTT at a concentration of 0.5 mg/mL was added and incubated for 4 h at 37 °C. Formazan crystals were added 100 μL of DMSO to each well. Absorbance was recorded at 540 nm on an Invitrologic microplate reader (Russia). Experiments for all compounds were repeated three times.

 doi:10.20944/preprints202309.1553.v1

2.3.2. Induction of Apoptotic Effects by test compounds. Flow Cytometry Assay

Cell Culture

HuTu 80 cells at 1×10^6 cells/well in a final volume of 2 mL were seeded into six-well plates. After 48 h of incubation, various concentrations of compounds **4b**, **5b**, **6a** and **8** were added to wells.

Cell Apoptosis Analysis

The cells were harvested at 2000 rpm for 5 min and, then, washed twice with ice-cold PBS, followed by resuspension in binding buffer. Next, samples were incubated with 5 μL of annexin V Alexa Fluor 647 (Sigma-Aldrich, USA) and 5 μL of propidium iodide for 15 min at room temperature in the dark. Finally, the cells were analyzed by flow cytometry (Guava easy Cyte, MERCK, USA) within 1 h. Experiments were repeated three times.

Mitochondrial Membrane Potential

Cells were harvested at 2000 rpm for 5 min and then washed twice with ice-cold PBS, followed by resuspension in JC-10 (10 μg/mL) and incubation at 37 °C for 10 min. Then, the cells were rinsed three times and suspended in PBS, the JC-10 fluorescence was observed by flow cytometry (Guava easy Cyte, MERCK, USA).

Detection of Intracellular ROS

HuTu 80 cells were incubated with compounds **4b**, **5b**, **6a** and **8** at $IC_{50}/2$ and IC_{50} concentrations for 48 hours. ROS generation was investigated using flow cytometry assay and CellROX® Deep Red flow cytometry kit. For this, HuTu 80 cells were harvested at 2000 rpm for 5 minutes and then washed twice with ice-cold PBS, followed by resuspension in 0.1 mL of medium without FBS, to which was added 0.2 μL of CellROX® Deep Red and incubated at 37 °C for 30 minutes After three times washing, cells and were suspended in PBS, and the cell production of ROS was immediately monitored, using a flow cytometer Guava easy Cyte, MERCK, USA).

ELISA Assay

HuTu 80 cells were incubated for 48 h with **4b**, **5b**, **6a** and **8** at $IC_{50}/2$ and IC_{50} concentrations. In vitro quantitative measurement of caspase-9 and caspase-8 was performed using ELISA kits (ELISA Kit for Caspase 9 (CASP9)-Human Cloud-Clone Corp.); ELISA Kit for Caspase 8 (CASP8)-Human-Cloud-Clone Corp. (CCC, Wuhan). The analysis was carried out according to the manufacturer's instructions. Samples were standardized for total protein content (1mg/ml). Protein concentration was determined with Coomassie-based assays using Bredford Dye Reagent (BIO-RAD, USA). The absorbance was measured using a microplate reader EPOCH (BioTek Instruments Inc. USA), at a wavelength of 450 ± 10 nm. Lysates of untreated HuTu 80 cells were used as controls.

Cell Cycle Analysis

The DNA content and cell-cycle distribution after compounds **4b**, **5b**, **6a** and **8** IC_{50} concentrations treatment were estimated by flow cytometry. After washing with PBS treated cells were suspended in 150 μl of PBS, then 0.5 ml phosphate-citrate buffer (0.05 M, pH 4.0) was added and the suspension was incubated at room temperature for 5min to facilitate the extraction of low molecular weight DNA. Following centrifugation the cells were resuspended in 150 μl DNA staining solution (20 μg/ml propidium iodide, 200 μg/ml DNase (RNase-free) and incubated in the CO_2 incubator (37 °C for 30 min). The distribution of the cell cycle was determined by fluorescence analysis of HuTu 80 cells stained with propidium iodide using Guava Easy Cyte (Guava easy Cyte, MERCK, USA) [65].

Hemolytic Assay

Hemolytic activity of Phosphonium salts was estimated by comparing the optical density of a solution containing the test compound with that of blood at 100% hemolysis. The experiments were carried out as described earlier [84].

 doi:10.20944/preprints202309.1553.v1

Antimicrobial Activity

Antimicrobial activity of test compounds was determined by serial microdilutions in 96-well plates using Mueller-Hinton broth for bacterial culture and Sabouraud broth for yeast culture. Cultures of gram-positive bacteria were used in the experiment: *Staphylococcus aureus* ATCC 6538 P FDA 209P, *Bacillus cereus* ATCC 10702 NCTC 8035, *Enterococcus faecalis* ATCC 29212; Gram-negative bacteria: *Escherichia coli* ATCC 25922, *Pseudomonas aeruginosa* ATCC 9027 and yeast: *Candida albicans* ATCC 10231, purchased from the State Collection of Pathogenic Microorganisms and Cell Cultures "SCPM-Obolensk". Methicillin-resistant strains of S. aureus (MRSA) were isolated from patients with chronic tonsillitis (MRSA-1) and sinusitis (MRSA-2) in the bacteriological laboratory of the Republican Clinical Hospital (Kazan, Russia). The experiments were carried out in triplicate.

Statistical Analysis

The IC_{50} values were calculated using the online calculator MLA – Quest Graph™ IC_{50} Calculator AAT Bioquest, Inc, February 23, 2022. Statistical analysis was performed using the Mann-Whitney test ($\rho < 0.05$). Tabular and graphical data contain averages and standard errors.

In vivo Study of Acute Toxicity of Aminophosphonic Salts

The study of acute toxicity was performed on males of outbred white mice of the CD-1 line at the age of 2-3 months weighing 20-30 grams. The total number of mice participating in the experiment was 200 individuals. Mice were obtained from the Research and Production Enterprise Laboratory Animal Farm based at the Branch of Shemyakin and Ovchinnikov Institute of Bioorganic Chemistry of the Russian Academy of Sciences (Pushchino). The animals were kept in accordance with [85–87] in standard conditions in a vivarium with 12 hours of daylight and free access to food and water. The animals were fed with complete feed made according to Specification (protein 22%, fiber 4% max., fat 5% max, ash 9% max, humidity 13.5% max, caloricvalue 295 kcal/100 g). The studies were conducted with a single parenteral – intraperitoneal (intra-peritoneal) injection, according to the method [87].

The substances were introduced in the form of solutions in 40% DMSO diluted in sterile saline solution. Solutions of substances were prepared immediately before administration. The total volume of the injected liquid was 0.1 ml / 10 g of animal weight. As a control, a group of mice was administered under similar conditions an equivalent amount (0.1 ml/ 10 g, or 10 ml/kg) of a solvent – 40% DMSO on sterile saline solution. The substances were administered in doses from 1 to 1000 mg/kg, there were 3-6 animals in each group. To assess acute toxicity, the animals were monitored 14 days after administration of the substance, assessing their general condition and recording deaths.

All animal experimentations and protocols were approved by the Local Ethics Committee of Kazan Federal University (Protocol № 4 dated 18 May 2017).

3. Results and discussion

3.1. Chemistry

3.1.1. Synthesis of Alkyl Diethylaminophoshonium salts

For the synthesis of the target aminophosphonium salts (APP) containing three, two or one diethylamine groups, we used hexaethyltriaminophosphine **1**, bis(tetraethyldiamino) phenylphosphine **2** and diethylaminodiphenylphosphine **3**, which were involved in the reactions with alkyl halides (C_6, C_8, C_9, C_{10}, C_{14}). There is information in the literature about the reaction of alkyl bromides C_6-C_{22} with the analog of the compound **1** – hexamethyltriaminophosphine [88,89], which was carried out without a solvent at 140-150 °C. Under hard conditions (130 °C), reactions of aminophosphin-1 with decyl chloride and a mixture of C_{16}-C_{18} bromides were also carried out [90]. Meanwhile, the data on the reaction of aminophosphine **1** with methyliodide [67] show that the process can proceed at room temperature. Taking into account the presented literature data, using the ^{31}P NMR method, we experimentally determined that the reactions of compounds **1**-**3** with alkyl iodides are carried out at room temperature in a polar solvent – acetonitrile (Scheme 2), and heating

Preprints (www.preprints.org) | NOT PEER-REVIEWED | Posted: 22 September 2023 doi:10.20944/preprints202309.1553.v1

is required for tetradecyl bromide in the same solvent. Quasi-phosphonium salts **4**-**6**, light yellow thick oils, were obtained with yields close to quantitative (see exp. part and Suppl Mater.). Only compound **6a** was obtained in a crystalline form.

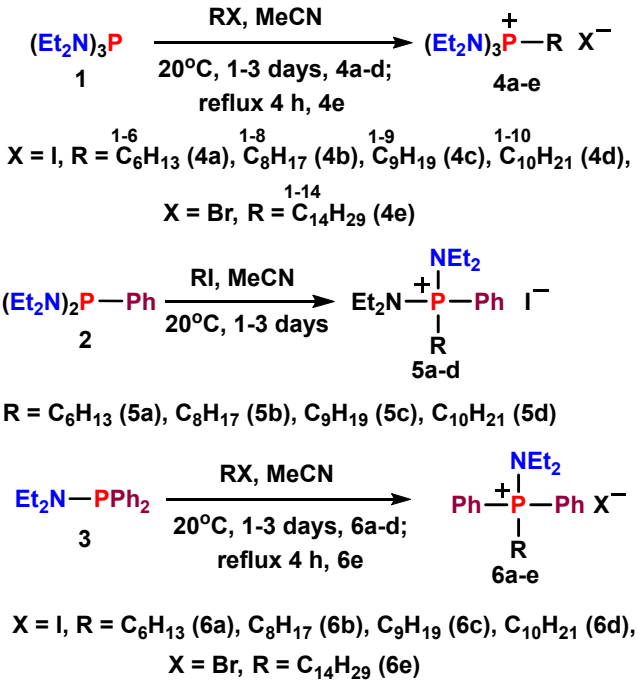

Scheme 2. Synthesis of Alkyl Diethylaminophoshonium salts.

The structure of all the compounds obtained was determined by ^{1}H, ^{13}C, ^{13}C-{^{1}H}, ^{13}C-{^{1}H}-dept, ^{31}P-{^{1}H} NMR, and the composition was confirmed by ESI mass spectroscopy and elemental analysis. It should be noted that the most characteristic for quasi-phosphonium structures **4**-**6** are chemical shifts in the ^{31}P-{^{1}H} NMR spectra. Depending on the number of amine groups, they are in two intervals – δ_P 58-59 ppm (**4**, **5**) and 51-52 ppm (**6**). In the NMR spectra of ^{13}C-{^{1}H} quasi-phosphonium salts **5**, **6** containing phenyl groups, the most characteristic is the position of the carbon resonance C^{i} (δ_C 119-123 ppm), and the values of the constants $^{1}J_{PC^i}$ are sensitive to the number of amino groups at the phosphonium center – 122-123 Hz (for **5**) and ~96.4 Hz (for **6**). It is interesting to note that the values of the constants $^{1}J_{PC^1}$ are also very sensitive to the number of amino groups: they are ~104.5 Hz (for **4**), 81-82 Hz (for **5**) and ~63.0 Hz (for **6**). The structure of compound **6a** was also proved by the XRD. Figure 1 shows the geometry of the molecule in a crystal. The phosphorus atom has a slightly distorted tetrahedral coordination, the valent angles near it vary from 106.76(6) to 115.35(6)°. The nitrogen atom has a strongly flattened pyramidal co-ordination, the sum of the valent angles near it is 356.0(1)°. The basic geometric parameters of the molecules (bond lengths and valent angles) are ordinary. A fragment of a hexyl substituent with a phosphorus atom P^{1}–C^{1}–C^{2}–C^{3} (up to the C^{4} atom) has a flat zigzag conformation (corresponding torsion angle –175.86(9)°), typical for paraffin crystals. Then a reversal occurs around the C^{3}–C^{4} bond: the torsion angle C^{2}–C^{3}–C^{4}–C^{5} is –67.4(2)°, and then the fragment C^{3}–C^{4}–C^{5}–C^{6} is also in a flat zigzag conformation (the corresponding torsion angle is 178.7(1)°).

Preprints (www.preprints.org) | NOT PEER-REVIEWED | Posted: 22 September 2023 doi:10.20944/preprints202309.1553.v1

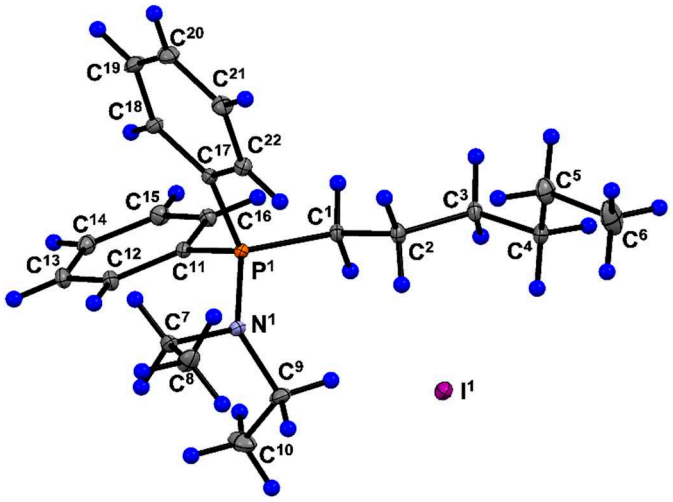

Figure 1. Geometry of molecule **6a** in crystal. Non-hydrogen atoms are shown in view of thermal ellipsoids with a probability of 50%. Hydrogen atoms are shown as spheres of arbitrary radius. Selected bond lengths (Å) and bond angles (deg): $P^1–N^1$ 1.634(1), $P^1–C^1$ 1.797(1), $P^1–C^{11}$ 1.802(1), $P^1–C^{17}$ 1.793(1), $N^1–P^1–C^1$ 110.64(6), $N^1–P^1–C^{11}$ 115.35(6), $N^1–P^1–C^{17}$ 106.83(5), $C^1–P^1–C^{11}$ 106.75(6), $C^1–P^1–C^{17}$ 109.67(6), $C^{11}–P^1–C^{17}$ 107.49(6).

In the crystal, the iodide anion has short C–H···I-type contacts with two neighboring phosphonium cations (Figure 2), and at the same time, a hexyl substituent approaches one of the phenyl substituents of the neighboring molecule. Apparently, the non-planar conformation of the hexyl substituent is determined by the steric reasons.

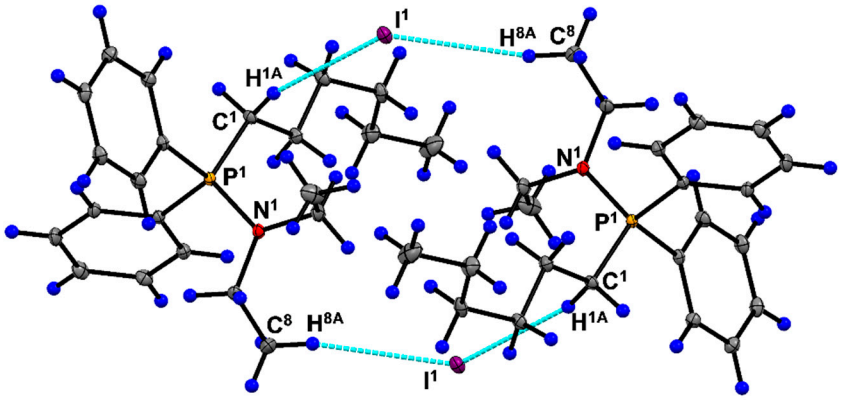

Figure 2. Short C–H···I-type contacts in crystal of compound **6a**.

For comparison with the data on the biological activity of compounds **4**-**6**, triethylammonium salt **7**, triphenylphosphonium salt **8** and 1,6-hexanediyl bis(hexaethyltriaminophosphonium)dibromide **9** (Scheme 3) were also obtained. The structure of these compounds is proved by NMR methods. It is interesting to note that the reaction of triphenylphosphine with octyl iodide in a solution of MeCN also proceeds already at room temperature and without heating (95 h, reagent concentration ~0.25 mol/l, conversion 71%). However, to accelerate the process, the reaction mass was heated for 1 h. We also carried out a competitive reaction of hexaethyltriaminophosphine **1** and triphenylphosphine with iodoctane in a solution of MeCN at room temperature. It turned out that the ratio of phosphonium salts **4b** and **8** after 24 hours of keeping the reaction mixture is 85 : 15, i.e., phosphine **1** has a higher reactivity. Since the rate-determining stage in the Arbuzov reaction is the nucleophilic attack of the P(III) atom on the electrophilic carbon atom of alkyl halide, it can be concluded that aminophosphine, despite the more electro-negative nitrogen atoms, is a stronger nucleophile compared to triphenylphosphine.

Preprints (www.preprints.org) | NOT PEER-REVIEWED | Posted: 22 September 2023 doi:10.20944/preprints202309.1553.v1

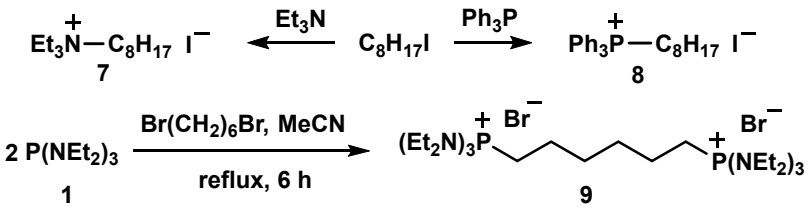

Scheme 3. Synthesis of ammonium salt **7**, phosphonium salt **8** and diphosphonium salt **9**.

3.1.2. Aminophosphonium Salt Decorated Liposomes and Solid Lipid Nanoparticles

Lipid nanosystems (liposomes and solid lipid nanoparticles) decorated by APP were obtained using widely used methods lipid film hydration method and high-pressure hot homogenization. The physicochemical characteristics are presented in Table 2. Previously, we found the optimal PC/cationic amphiphile ratio = 99.8/0.2 for obtaining liposomal nanosystems with a positively charged surface [91,92] and SLN [65].

Table 2. Characteristics of lipid systems PC-liposomes and solid lipid nanoparticles (SLN), average particle size ($Z_{average}$, nm), polydispersity index (PDI), Zeta potential (ξ, mV), 25 °C.

Composition	Ratio, (% w/w)	$Z_{average}$, nm	PDI	ξ, mV
PC [75,76]	100	119±2	0.12±0.02	−7.0±2
PC/**4a**	99.8/0.2	121±0.5	0.09±0.01	−5.1±0.2
PC/**4b**	99.8/0.2	124±1	0.07±0.01	+4.3±0.4
PC/**4c**	99.8/0.2	125±1	0.14±0.02	+9.3±0.3
PC/**4d**	99.8/0.2	134±1	0.14±0.01	+13.9±0.4
PC/**4e**	99.8/0.2	115±1	0.12±0.01	+26.8±3
PC/**5b**	99.8/0.2	129±1	0.14±0.01	+3.2±0.3
PC/**5c**	99.8/0.2	116±2	0.11±0.01	+7.1±0.2
PC/**5d**	99.8/0.2	126±0.5	0.14±0.02	+13.3±0.5
PC/**4d**-Rhod	99.8/0.2	122±0.2	0.11±0.01	+19.0±1.7
PC/**5b**-Rhod	99.8/0.2	116±0.5	0.10±0.02	+7.9±0.2
PC/**5c**-Rhod	99.8/0.2	118±0.3	0.09±0.03	+2.6±0.3
PC/**5d**-Rhod	99.8/0.2	117±0.4	0.1±0.01	+14.2±0.6
PC/**5d**-Rhod*	99.8/0.2	115±0.2	0.1±0.01	−8.4±0.6
PC/**8**	99.8/0.2	117±0.5	0.12±0.02	+16.3±2.5
PC/**7**	99.8/0.2	124±0.1	0.15±0.01	−11.7±1.6
SLN [65]	100	104±1	0.24± 0.01	−17.2±1
SLN/**4b**	99.3/0.7	108±0.3	0.31±0.04	−15.6±0.5
SLN/**5b**	99.3/0.7	114±1	0.24±0.01	−15.8±0.7
SLN/**5c**	99.3/0.7	132±2	0.32±0.03	−7.7±0.5
SLN/**5d**	99.3/0.7	147±2	0.47±0.02	−3.6±0.1
SLN-Cur	100	125±1	0.2±0.01	−28.0±1
SLN/**5d**-Cur	99.8/0.2	123±1	0.21±0.01	−18.5±1

*6 month storage.

The size of lipid nanoparticles is close to 100 nm. The polydispersity index is not higher than 0.15 for liposomal systems. The zeta potential (ζ) of liposomal systems decorated with aminophosphonium salts 4 and 5 varies from neutral to positive values (Figure 3). This indicates the modification of nanoparticle surface. Linearity (r^2 = 0.995 and r^2 = 0.991) of ζ change is observed with increasing length of alkyl chain of aminophosphonium salts (n) from n = 6 to n = 14 for **4** and from n = 6 to n = 10 for **5**. This tendency does not depend on substituents at the phosphorus atom of amino-phosphonium salts (monoaminophosphonium and diaminophosphonium derivatives). The same

Preprints (www.preprints.org) | NOT PEER-REVIEWED | Posted: 22 September 2023 doi:10.20944/preprints202309.1553.v1

tendency is observed for SLN/**5**. The surface charge of SLN changes from negative to positive values with linearity $r^2 = 0.983$ (Figure 3). This indicates the modification of nanoparticles with phosphonium salts. An increase the polydispersity index and the forming of smaller nanoparticles close to 20 nm occurs with an increase in the alkyl chain for SLN/**5**. SLN/**4c** and SLN/**4d** systems were not stable at the pre-emulsion preparation stage. Therefore, only SLN/**4b** and SLN/**5b** were used for in vitro studies.

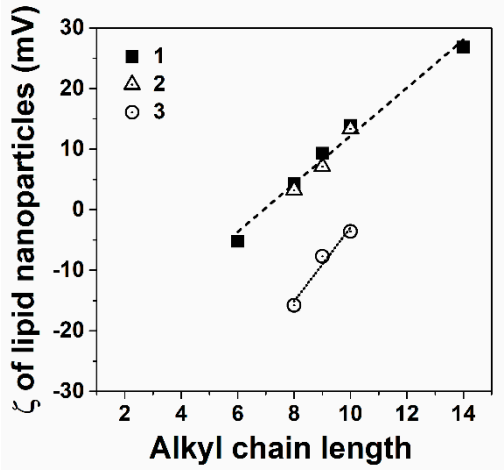

Figure 3. The zeta potential of liposomes (1, 2) and solid lipid nanoparticles (3) decorated with of aminophosphonium salts **4** (1) and **5** (2, 3) with different alkyl chain lengths.

The release of water-soluble dye rhodamine B from liposomes was studied to evaluate the release time of encapsulated drugs from liposomes and the rigidity of the phospholipid membrane. The release of rhodamine B from PC liposomes and liposomes modified with aminophosphonium salts is shown in Figure 4. Modification of liposomes with aminophosphonium salts does not affect the release of dye from liposomal systems. 50% of rhodamine B is released within 8 hours, complete release occurs within more than 70 hours.

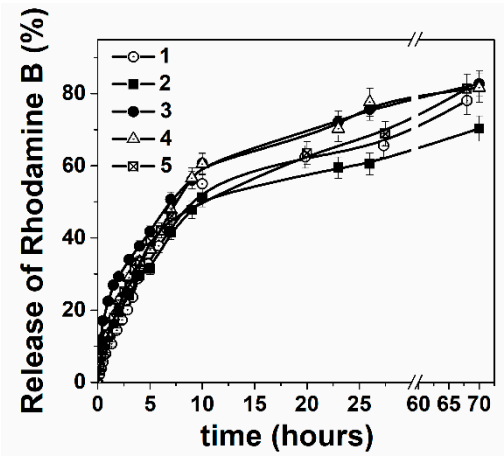

Figure 4. Release profile of Rhodamine B from PC-liposomes (1) and P^+-PC-liposomes modified by aminophosphonium salt **4d** (2), **5b** (3), **5c** (4) and **5d** (5), (n = 3, 3 times were replicated), phosphate buffer (0.025 M), pH 7.4, 37 °C.

Preprints (www.preprints.org) | NOT PEER-REVIEWED | Posted: 22 September 2023 doi:10.20944/preprints202309.1553.v1

3.2. Biology

3.2.1. Cytotoxic Effects of Aminophosphonium salts

In primary studies, in vitro cell models of cancer and normal cell lines are widely used to evaluate the direct cytotoxic effect of the new chemical compounds proposed as potential drugs. Table 1 presents data on the cytotoxicity of aminophosphonium salts derivatives tested against a wide panel of human cancer and normal cell lines. The results are characterized by the values of the concentrations of semi-maximal inhibition of IC_{50}, as well as the data of the selectivity index (SI), calculated as the ratio between the value of IC_{50} for normal cells and the value of IC_{50} for cancer cells. Most of the compounds demonstrated a high and moderate activity with respect to the entire spectrum of the cell lines used in the experiments. However, in some cases, the cytotoxicity of the tested compounds against normal cells was lower compared to cancer cells. At the same time, the selectivity index was SI ≥ 10, which indicates their high selectivity [93].

Most of the studied compounds generally exhibit a high cytotoxicity against the M-Hela cell line. So, for compounds **4b-e**, **5b-d**, **6b-e**, the IC_{50} is in the range 0.24-1.8 μM (SI 1.6-17). At the same time, compounds **4d** (SI 7.1), **6a** (SI 4.8) and **6b** (SI 17) are distinguished by the SI indicator, compound **6b** being a leader, whose IC_{50} is two times lower than that of doxorubicin.

On the HuTu 80 cell line, a pronounced dependence of SI on the aminophosphonium cation is observed: at a rather low IC_{50} value of 0.06-4.0 μM for compounds **4**-**6** (for compounds **4e** and **6e**, IC_{50} is 3 times lower than for doxorubicin), the selectivity index increases in a row **4** < **5** < **6**. Thus, among triaminophosphonium compounds, the maximum value is observed for salt **4e** (SI 28), among diaminophosphonium compounds – for salt **5a** (SI 210), among monoaminophosphonium derivatives, the maximum index is shown for compound **6a** (SI 277). In the series of aminophosphonium salts **6**, two more derivatives have good indices – **6b** (SI 81) and **6c** (SI 42). A similar picture is realized for the PC3 cell line, the growth of which is rather selectively inhibited by compounds **6b**, **6c** and **6a** with the following values of IC_{50} (μM) and SI: 0.085±0.07 (19), 1.0±0.08 (8.3), and 4.0±0.3 (6.9). Among diaminophosphonium compounds, only salt **5a** (4.9±0.4 μM, SI 13) exhibits selectivity, whereas in the series of derivatives **4** there are no compounds with high SI values.

Monoaminophosphonium compounds **6a-c**, **e** also showed higher efficiency for the Du-145 cell line compared to derivatives **4** and **6** with the following IC_{50} (μM) and SI values: **6b**, 0.8±0.07 (20); **6a**, 2.6±0.3 (11); **6e**, 0.4±0.02 (7.0); **6c**, 1.3±0.1 (6.4). Among tri- and diaminophosphonium compounds, **4d**, **4c** and **5c** with values IC_{50} (μM) and SI can be noted: 1.2±0.1 (10), 0.4±0.03 (4.3), 0.9±0.07 (4.6). The trends found are also observed on the PANC-1 cell line: here the most effective compounds are **6b**, **6e**, **6c**, **6a**, **4e**, **4c**, which have the following values of IC_{50} (μM) and SI (given in order of decreasing SI): **6b**, 1.3±0.1 (12); **6e**, 0.3±0.02 (9.3); **4d**, 1.6±0.1 (7.5); **6c**, 1.3±0.1 (6.4); **6a**, 5.5±0.4 (5.50); **4e**, 0.4±0.03 (4.3).

The studied compounds also showed a moderate or high cytotoxicity on the MCF-7 cell line. In a series of compounds with three amino groups at the phosphorus atom, compound **4e** showed the highest cytotoxicity (IC_{50} 0.9±0.07 μM, SI 1.7). Compound **4d** (IC_{50} 2.1±0.2 μM) showed a high selectivity index (SI 5.7). The replacement of one or two amino groups with a phenyl substituent in compounds **5b-d**, **6c-e**, did not lead to an increase in cytotoxicity with respect to MCF-7 cell line, which was 0.7-4.2 μM (SI 2). Cytotoxicity (IC_{50}, μM) and SI of octyltriphenylphosphonium iodide **8** (4.2±0.3, 2.2) were comparable with the activity of compound **6c**.

For the A549 cell line, only the activity of compound **5a** can be noted, which, with lower efficiency (IC_{50} 17.0±0.3 μM, SI 3.7), is 157 times less toxic in relation to the normal WI38 cell line compared with doxorubicin (IC_{50} 0.7±0.06 ±M, ns).

The analysis of IC_{50} and SI allows making a preliminary conclusion about the more pronounced cytotoxicity and higher SI values of monoaminophosphonium derivatives **6** compared with tri- and diamino-substituted phosphonium salts **4** and **5** on HuTu 80, PC3 and Du-145 cell lines. The influence of the length of the alkyl substituent in amiphosphonium derivatives is expressed in an increase in cytotoxicity towards cancer cells when moving from derivatives with a smaller alkyl radical to larger

Preprints (www.preprints.org) | NOT PEER-REVIEWED | Posted: 22 September 2023 doi:10.20944/preprints202309.1553.v1

ones. This is most clearly noticeable in the transition from C_6 to C_8 (IC_{50} **4b** > **4a** 50.6 μM for M-HeLa), **5b** > **5a** (ΔIC_{50} 21.2 μM for M-HeLa), **6b** > **6a** (ΔIC_{50} 4.9 μM for M-HeLa).

In vitro cytotoxicity was studied for nanotherapeutic forms (liposomes and SLN) of compounds **4**, **5b-5d**, **7** and **8**. Lipid systems for **4b-d** and **5b-d** exhibit improved cytotoxic activity against tumor cells (except SK-OV-3) compared to individual compounds (Figures 5 and 6). The maximum difference is observed for SLN/**4b**, where the cytotoxicity 4 times (M-HeLa) and 40 times (PC3) better than for **4b**. The IC_{50} for lipid systems PC/**4c**, PC/**4d**, PC/**5b**, PC/**5c**, PC/**5d** and SLN/**4b** is lower than for the reference drug DOX. At the same time, all lipid nanoforms are less toxic toward to normal cell lines. Maximum selectivity SI = 53 and SI = 56 is achieved in the case of SLN/**4b** against cell lines MCF-7 and DU-145, respectively. The maximum SI is observed for PC/**4c** and PC/**4e**, the SI values are SI = 30 and 24 for the MCF-7 cell line and SI = 22.8 for DU-145, as well as PC/8, where SI = 36 and 24 against cell lines A549 and T98G.

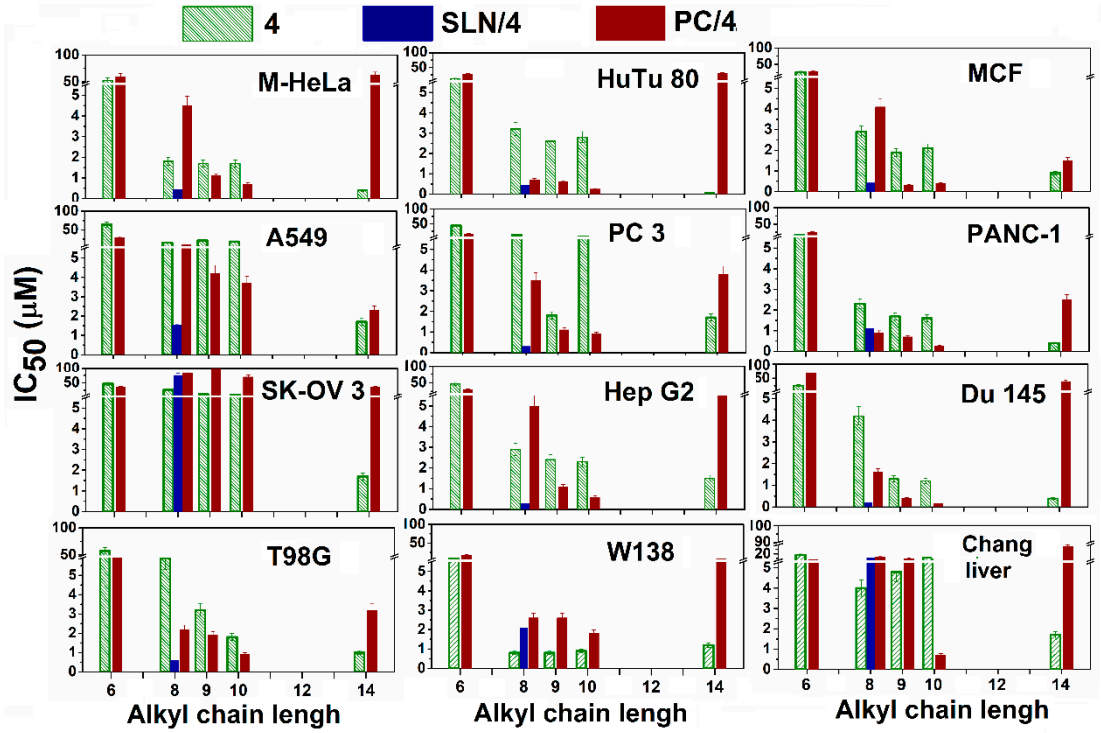

Figure 5. Summarized results showing the IC_{50} for compounds **4** with different alkyl chain length and lipid formulations SLN/**4** and PC/**4**-liposomes in cancer cells and normal cells after 24 h of incubation.

Preprints (www.preprints.org) | NOT PEER-REVIEWED | Posted: 22 September 2023 doi:10.20944/preprints202309.1553.v1

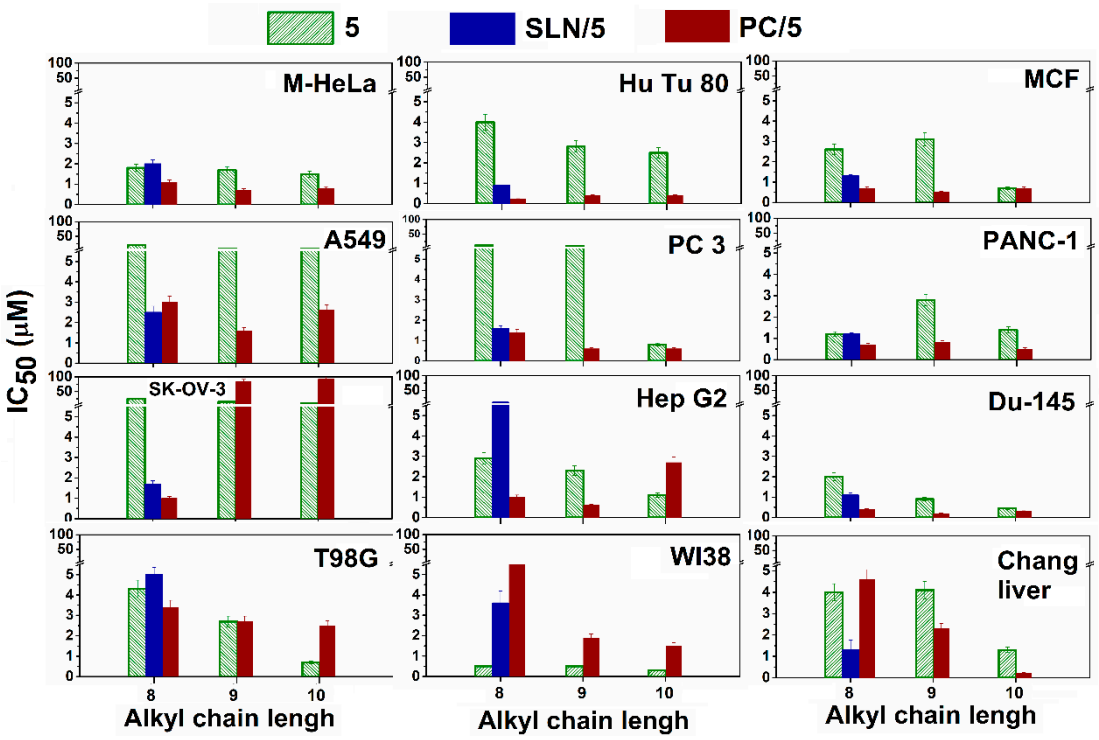

Figure 6. Summarized results showing the IC_{50} for compounds **5** with different alkyl chain length and and lipid formulations SLN/**5** and PC/**5**-liposomes in cancer cells and normal cells after 24 h of incubation.

It should be noted that the activity of PC/4 improves with an increase alkyl chain length from the hexyl to the decyl derivatives in the range of 8÷456 times, in contrast to PC/**5**. There is no change in activity depending on the length of alkyl chain for the PC/**5**. Interestingly, the surface charge of both PC/**4** and PC/**5** liposomes changes linearly with increasing length of the alkyl chain (Figure 3) and does not depend on the substituent at the phosphorus atom. Consequently, biological activity is not linearly related to the charge of liposomal systems, but depends mainly on the nature of substituent at the phosphorus atom. In addition, SLN/**4b** exhibits improved biological activity compared to both SLN/**5b** and PC/**4b** liposomal systems, which also indicates the influence of the nature of the substituent at the phosphorus atom.

3.2.2. Cellular uptake of liposomes and SLN modified by aminophosphonium salts

Dye-labeled (rhodamine and curcumin) liposomes and SLN, respectively, were prepared to visualize P^+-lipid nanoparticles and confirm their internalization by cells. The characteristics are presented in Table 3. As we see on Figure 7 rhodamine-labeled liposomes and curcumin-labeled SLN were located in the cytoplasm after 1 hour their incubation with cells. That indicates that the nanoparticles were internalized by tumor cells.

Table 3. Cytotoxic Effects (IC_{50}, μM) and selectivity index values (SI) of aminophosphonium salts and their lipid formulations (liposomes and SLN) (MTT assay, 48 h).

Test compounds	Cancer cell lines										Normal cell lines	
	M-HeLa	MCF-7	HuTu 80	PANC- 1	A549	PC3	T98G	Hep G2	SK-OV-3	DU-145	WI38	Chang liver
4a	52.4±3.7 (ns)	26.0±1.8 (ns)	11.4±0.9 (1.6^b)	16.1±1.3 (1.1^b)	64.1±4.5 (ns)	44.0±3.1 (ns)	57.4±4.0 (ns)	46.6±3.3 (ns)	46.6±3.5 (ns)	26.2±1.9 (ns)	7.6±0.6	17.7±1.5
PC/4a	60±12 (ns)	28.3±2.0 (ns)	26.1±1.8 (ns)	24.6±1.6 (ns)	29.2±1.9 (ns)	15.5±1.2 (ns)	37.3±2.8 (ns)	29.1±2.3 (ns)	35.5±2.5 (ns)	68.5±4.1 (ns)	17.2±2.4	6.5±0.8
4b	1.8±0.1 (2.2^b)	2.9±0.2 (1.4^b)	3.2±0.2 (1.3^b)	2.3±0.1 (1.7^b)	15.4±1.2 (ns)	11.6±0.9 (ns)	5.9±0.4 (ns)	2.9±0.2 (1.4^b)	26.3±1.8 (ns)	4.2±0.3 (ns)	0.8±0.06	4.0±0.3
PC/4b	4.5±0.3 (2.8^b)	4.1±0.3 (3.1^b)	0.7±0.06 (18^b)	0.9±0.08 (14^b)	9.5±0.8 (1.3^b)	3.5±0.4 (3.6^b)	2.2±0.1 (5.7^b)	5.0±0.4 (2.5^b)	83.0±5.8 (ns)	1.6±0.1 (8.0^b)	2.6±0.1	12.6±1.2
SLN/4b	0.42±0.04 (26^b)	0.21±0.02 (53^b)	0.42±0.04 (26^b)	1.1±0.1 (10^b)	1.5±0.1 (7.4^b)	0.3±0.03 (37^b)	0.6±0.06 (19^b)	0.3±0.03 (37^b)	75±6 (ns)	0.2±0.01 (56^b)	2.1±0.2	11.1±1.2
4c	1.7±0.1 (2.8^b)	1.9±0.1 (2.5^b)	2.6±0.2 (1.8^b)	1.7±0.1 (2.8^b)	21.1±1.5 (ns)	1.8±0.1 (2.7^b)	3.2±0.2 (1.5^b)	2.4±0.1 (2.0^b)	12.1±1.1 (ns)	1.3±0.1 (ns)	0.8±0.07	4.8±0.4
PC/4c	1.1±0.09 (ns)	0.3±0.02 (30^b)	0.6±0.05 (15.6^b)	0.7±0.06 (13^b)	4.2±0.3 (2.2^b)	1.1±0.08 (8.3^b)	1.9±0.1 (4.8^b)	1.1±0.08 (8.3^b)	99±7 (ns)	0.4±0.03 (22.8^b)	2.6±0.2	9.1±0.8
4d	1.7±0.1 (7.1^b)	2.1±0.2 (5.7^b)	2.8±0.2 (4.3^b)	1.6±0.1 (7.5^b)	18.4±1.3 (ns)	7.3±0.6 (1.6^b)	1.8±0.2 (6.7^b)	2.3±0.1 (5.2^b)	10.0±0.9 (1.2^b)	1.2±0.1 (10^b)	0.9±0.08	12.0±0.9
PC/4d	0.7±0.06 (2.6^a)	0.4±0.03 (4.5^a)	0.24±0.02 (7.5^a)	0.26±0.02 (7.0^a)	3.7±0.3 (ns)	0.9±0.08 (2.0^a)	0.9±0.07 (2.0^a)	0.6±0.05 (3.0^a)	69.4±4.9 (ns)	0.15±0.01 (12^a)	1.8±0.1	0.7±0.06
4e	0.4±0.03 (4.3^b)	0.9±0.07 (1.9^b)	0.06±0.005 (28^b)	0.4±0.03 (4.3^b)	1.7±0.1 (1.0^b)	1.7±0.1 (1.0^b)	1.0±0.09 (1.7^b)	1.5±0.1 (1.1^b)	1.7±0.1 (1.0^b)	0.4±0.03 (4.3^b)	1.2±0.1	1.7±0.1
PC/4e	62±5.3 (ns)	1.5±0.8 (24^b)	29.7±2.4 (1.2^b)	2.5±0.3 (14^b)	2.3±0.1 (16^b)	3.8±0.3 (9.5^b)	3.2±0.2 (11^b)	7.9±0.6 (4.5^b)	35.5±2.8 (1^b)	38.5±3.2 (ns)	7.1±0.7	36.0±2.9
5a	23.0±1.6 (2.7^a)	17.1±1.3 (3.7^a)	0.3±0.02 (210^a)	17.8±1.4 (3.5^a)	17.0±1.3 (3.7^a)	4.9±0.4 (13^a)	30.3±2.1 (3.7^a)	16.5±1.3 (3.8^a)	20.0±1.6 (3.2^a)	6.3±0.5 (10^a)	63.0±4.4	22.6±1.6
5b	1.8±0.1 (2.2^b)	2.6±0.2 (1.5^b)	4.0±0.3 (1.0^b)	1.2±0.1 (3.3^b)	20.0±1.6 (ns)	11.4±0.9 (ns)	4.3±0.3 (1.0^b)	2.9±0.3 (1.4^b)	25.6±1.8 (ns)	2.0±0.1 (2.0^b)	0.5±0.4	4.0±0.3
PC/5b	1.1±0.08 (5.5^a)	0.7±0.06 (8.6^a)	0.22±0.01 (5.5^a)	0.7±0.06 (8.6^a)	3.0±0.2 (2.0^a)	1.4±0.1 (4.3^a)	3.4±0.2 (1.8^a)	1.0±0.09 (6.0^a)	1.8±0.1 (3.3^a)	0.4±0.03 (15^a)	6.0±0.5	4.6±0.4
SLP/5b	2.0±0.1	1.3±0.1	0.9±0.07	1.2±0.1	2.5±0.2	1.6±0.1	5.0±0.4	10.0±0.9	1.7±0.1	1.1±0.09	3.6±0.2	1.3±0.1

doi:10.20944/preprints202309.1553.v1

	(1.8[a])	(2.8[a])	(4.0[a])	(3.0[a])	(1.4[a])	(2.3[a])	(ns)	(ns)	(2.1[a])	(3.3[a])		
5c	1.7±0.1 (2.4[b])	3.1±0.2 (1.3[b])	2.8±0.3 (1.5[b])	2.8±0.2 (1.5[b])	8.7±0.7 (ns)	10.0±0.9 (ns)	2.7±0.3 (1.5[b])	2.3±0.1 (1.8[b])	14.8±1.2 (ns)	0.9±0.07 (4.6[b])	0.5±0.4	4.1±0.3
PC/5c	0.7±0.06 (3.3[b])	0.5±0.04 (4.6[b])	0.4±0.03 (5.8[b])	0.8±0.06 (2.9[b])	1.6±0.1 (1.4[b])	0.6±0.05 (3.8[b])	2.7±0.2 (ns)	0.6±0.05 (3.8[b])	83.1±5.8 (ns)	0.2±0.01 (12[b])	1.9±0.1	2.3±0.1
5d	1.5±0.1 (ns)	0.7±0.06 (1.9[b])	2.5±0.1 (ns)	1.4±0.1 (ns)	8.9±0.7 (ns)	0.8±0.06 (1.6[b])	0.7±0.05 (1.9[b])	1.1±0.09 (1.2[b])	10.0±0.8 (ns)	0.45±0.03 (2.9[b])	0.3±0.02	1.3±0.1
PC/5d	0.8±0.07 (1.9[a])	0.7±0.06 (2.1[a])	0.4±0.02 (3.8[a])	0.5±0.04 (3.0[a])	2.6±0.2 (ns)	0.6±0.05 (2.5[a])	2.5±0.2 (ns)	2.7±0.2 (ns)	92.4±6.5 (ns)	0.3±0.02 (5.0[a])	1.5±0.1	0.23±0.01
6a	5.8±0.4 (4.8[a])	17.0±1.3 (1.6[a])	0.1±0.007 (277[a])	5.5±0.4 (5.0[a])	48.2±3.4 (ns)	4.0±0.3 (6.9[a])	18.4±1.5 (1.5[a])	34.4±2.4 (ns)	36.8±2.6 (ns)	2.6±0.3 (11[a])	27.7±1.9	15.2±1.3
6b	0.95±0.08 (17[a])	9.5±0.8 (1.7[a])	0.2±0.01 (81[a])	1.3±0.1 (12[a])	13.0±1.1 (1.2[a])	0.85±0.07 (19[a])	3.4±0.2 (5.0[a])	11.6±0.9 (1.4[a])	17.6±1.4 (ns)	0.8±0.07 (20[a])	16.1±1.2	0.42±0.03
6c	0.9±0.07 (1.6[a])	4.2±0.3 (2.0[a])	0.2±0.01 (42[a])	1.3±0.1 (6.4[a])	11.4±0.9 (ns)	1.0±0.08 (8.3[a])	2.4±0.1 (3.5[a])	6.2±0.5 (1.3[a])	12.7±1.1 (ns)	1.3±0.1 (6.4[a])	8.3±0.7	0.5±0.04
6d	0.24±0.02 (1.6[a])	1.6±0.1 (ns)	0.35±0.02 (1.1[a])	0.4±0.03 (1.0[a])	8.2±0.7 (ns)	1.4±0.1 (ns)	0.6±0.05 (ns)	1.3±0.1 (ns)	3.9±0.4 (ns)	0.43±0.03 (1.0[a])	0.4±0.03	0.3±0.02
6e	0.4±0.03 (7.0[a])	1.2±0.1 (2.3[a])	0.07±0.005 (40[a])	0.3±0.02 (9.3[a])	2.1±0.1 (1.3[a])	1.5±0.1 (1.9[a])	1.1±0.09 (2.5[a])	1.4±0.1 (2.0[a])	1.6±0.1 (1.8[a])	0.4±0.02 (7.0[a])	2.8±0.2	2.5±0.2
7	16.1±1.3 (3.0[a])	29.1±2.0 (1.7[a])	1.9±0.2 (26[a])	44.6±3.1 (1.1[a])	>100 (ns)	32.7±2.3 (1.5[a])	>100 (ns)	>100 (ns)	69.0±4.8 (ns)	58.0±4.1 (ns)	49.0±3.4	34.0±2.4
PC/7	148±12 (ns)	67±5.4 (ns)	54.3±3.8 (ns)	134.2±10 (ns)	>100 (ns)	41.7± (ns)	>100 (ns)	>100 (ns)	>100 (ns)	99.2± (ns)	12.6±1.3	0.3±0.02
8	0.45±0.04 (20[a])	4.2±0.3 (2.2[a])	0.09±0.006 (102[a])	0.3±0.02 (31[a])	8.7±0.7 (1.1[a])	0.4±0.03 (23[a])	0.6±0.05 (15[a])	1.6±0.1 (5.8[a])	9.8±0.7 (ns)	0.4±0.03 (23[a])	9.2±0.8	3.0±0.2
PC/8	17.0±1.5 (1.7[b])	11.2±0.9 (2.6[b])	6.2±0.5 (4.7[b])	18.2±1.4 (1.6[b])	0.8±0.06 (36[b])	35.6±2.2 (ns)	1.2±0.1 (24[b])	37.2±2.5 (ns)	67.0±4.7 (ns)	2.5±0.1 (12[b])	28.0±1.8	29.0±2.0
9	31.1±3.9 (1.5[a])	37.8±4.8 (1.2[a])	13.1±1.7 (3.5[a])	39.6±5.1 (1.2[a])	>100	34.9±4.5 (1.3[a])	>100	53.9±6.9 (ns)	36.4±4.7 (1.3[a])	50.5±6.4 (ns)	45.8±5.9	37.2±4.8
doxorubicin	2.1±0.1 (ns)	0.4±0.03 (1.3[b])	0.2±0.01 (2.5[b])	2.2±0.1 (ns)	0.7±0.06 (ns)	1.4±0.1 (ns)	1.0±0.09 (ns)	0.2±0.01 (2.5[b])	6.7±0.5 (ns)	0.3±0.02 (1.7[b])	0.4±0.03	0.5±0.03

The experiments were performed in triplicate. Results are expressed as the mean ± standard deviation (SD); nd – not done; ns – no selectivity. [a]The selectivity index was calculated relative to the cell line WI38. [b]The selectivity index was calculated relative to the cell line Chang liver.

doi:10.20944/preprints202309.1553.v1

Preprints (www.preprints.org) | NOT PEER-REVIEWED | Posted: 22 September 2023 doi:10.20944/preprints202309.1553.v1

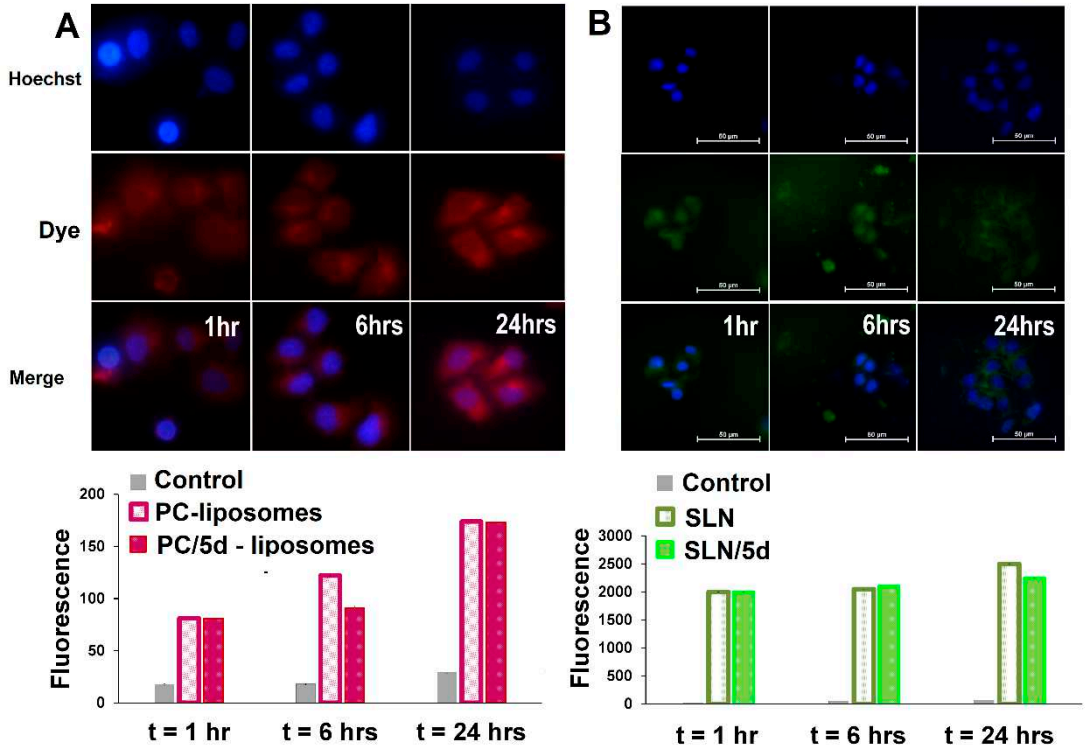

Figure 7. Confocal microscopic images and cellular uptake study (A) Rhodamine B labelled-PC/**5d**-liposomes, (B) curcumin labelled SLN/**5d** after incubation time (t = 0, 1, 6 and 24 hours).

3.2.3. Apoptosis assay

One of the important properties of cancer cells is their ability to avoid drug-induced apoptosis [94,95]. At the same time, the resistance of cancer cells increases both to the conventional antitumor therapy (chemotherapy, radiation therapy) and to the alternative therapeutic drugs [96]. Overcoming resistance by reactivating apoptosis is the main direction of the search for promising cancer treatment methods [97,98]. Effective induction of apoptosis using new therapeutic drugs may be an important strategy for preventing cancer recurrence and metastases [99]. The creation of drugs in this field is a difficult task, since the process of apoptosis is complicated by various resistance mechanisms and a multifaceted connection with cross-molecular pathways [100]. The main directions of development in recent decades include the design and synthesis of compounds inhibiting anti-apoptotic and activating pro-apoptotic pathways [101]. For the successful introduction of new molecules, it is necessary to study the fundamental molecular mechanisms of apoptosis and careful design of innovative drugs. In this regard, the apoptosis-inducing properties of various representatives of aminophosphonium salts **4b**, **5b**, **6a** and **8** with high cytotoxicity and selectivity against the HuTu 80 cancer cell line were investigated. The experiments were carried out by the flow cytometry at concentrations of $IC_{50}/2$ and IC_{50} (Figure 8). It can be seen that in HuTu 80 cells, after 48-hour incubation in the presence of compounds **4b** and **5b**, dose-dependent apoptosis was observed with a predominance of apoptotic effects in the late stage. For monoaminophosphonium salt **6a**, the number of necrotic cells prevailed at both concentrations, while for triarylphosphonium salt **8**, the apoptosis-inducing effect was more active in the early stage of apoptosis. The results obtained indicate the influence of structural modifications of aminophosphonium salts on the process of apoptosis in HuTu 80 cells.

Preprints (www.preprints.org) | NOT PEER-REVIEWED | Posted: 22 September 2023 doi:10.20944/preprints202309.1553.v1

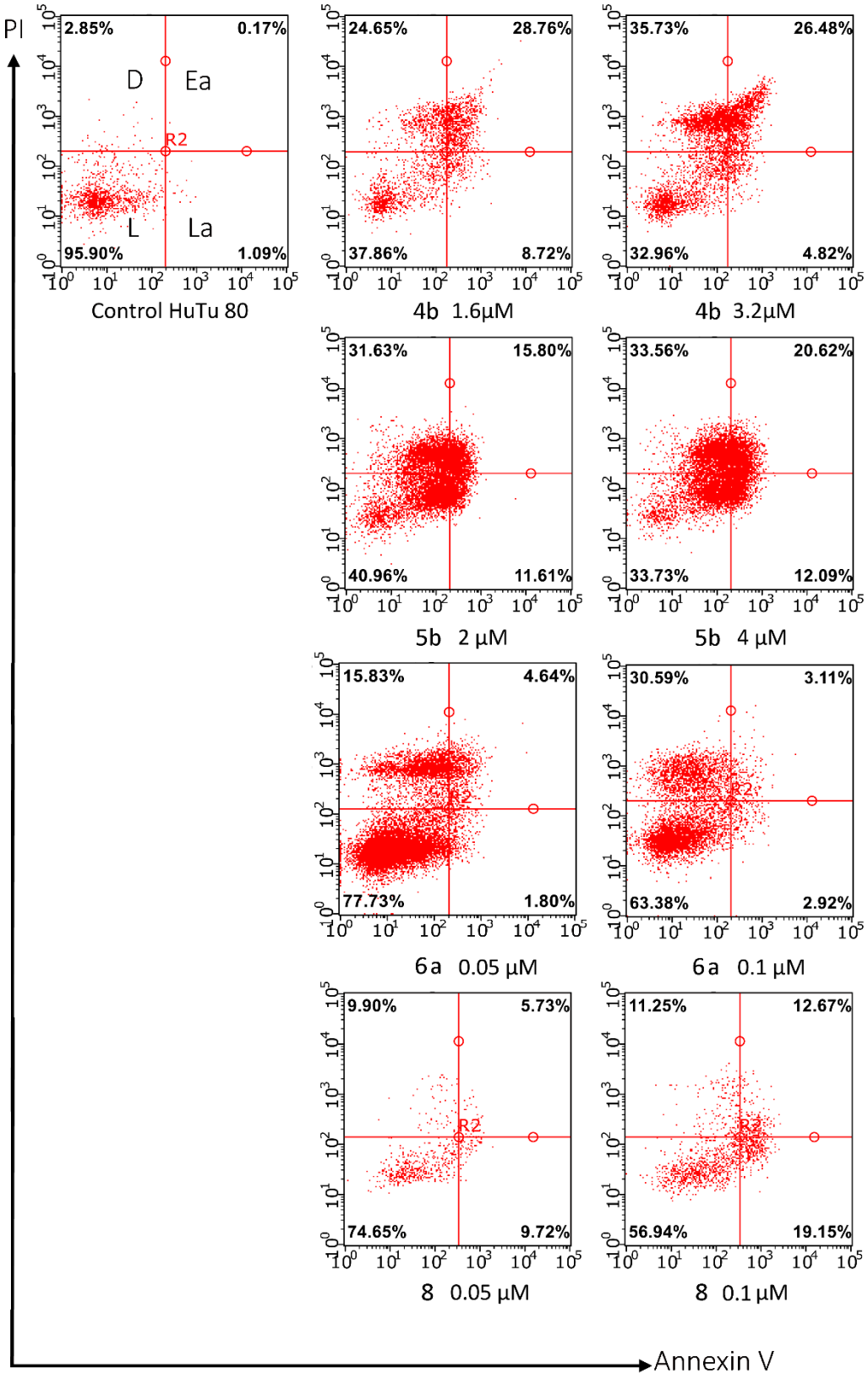

Figure 8. Induction of apoptosis in HuTu 80 cells incubated with compounds **4b**, **5b**, **6a** and **8** at concentration $IC_{50}/2$ and IC_{50}; L – living cells; D – dead cells; Ea. – early apoptotic cells; La. – late apoptotic cells.

Preprints (www.preprints.org) | NOT PEER-REVIEWED | Posted: 22 September 2023 doi:10.20944/preprints202309.1553.v1

3.2.4. Effect of Aminophosphonium salts on mitochondrial potential

Most forms of apoptosis in mammals are realized not through cell death receptors, but through the mitochondrial pathway. In this case, the outer membrane of the mitochondria breaks, and soluble proteins of the intermembrane space enter the cytoplasm. The permeability of the outer membrane of mitochondria is a finely regulated process, and its increase is a key event in triggering apoptosis. Induction of apoptosis by compounds **4b**, **5b**, **6a** and **8** at concentrations of $IC_{50}/2$ and IC_{50} via the mitochondrial pathway on the HuTu 80 cell line was studied by flow cytometry using fluorescent dye JC-10 from the Mitochondria Membrane Potential Kit [64].

JC-10 accumulates in the mitochondrial matrix and forms aggregates (J-aggregates) with red fluorescence in normal cells with a high mitochondrial membrane potential. A decrease in the mitochondrial membrane potential of HuTu 80 cells was observed after 48-hour treatment with compounds **4b**, **5b**, **6a** and **8** (Figure 9). Compounds **6a** and **8** have been shown to cause a more significant decrease in the mitochondrial membrane potential in HuTu 80 cells compared to **4b** and **5b**. For all compounds, the effect of membrane depolarization is noticeably enhanced in the IC_{50} concentration. The obtained results suggest that the mechanism of cytotoxic action of **4b**, **5b**, **6a** and **8** may proceed along the internal mitochondrial apoptotic pathway.

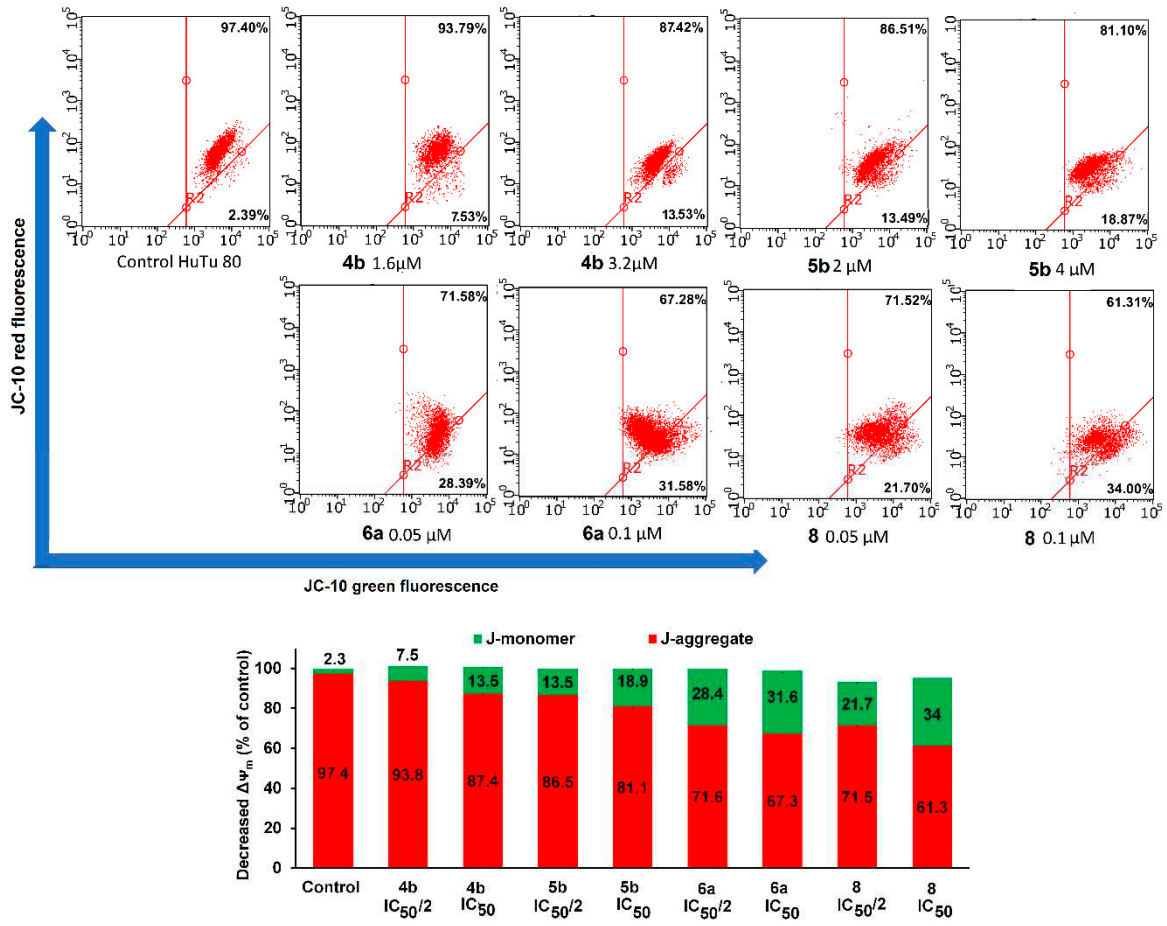

Figure 9. Effects on the mitochondrial membrane potential by **4b**, **5b**, **6a** and **8** at concentrations $IC_{50}/2$ and IC_{50} in HuTu 80 cells.

3.2.5. Effect of Aminophosphonium salts on ROS level in cancer cells

Evaluation of the production of reactive oxygen species (ROS) by the tested compounds complements the data on their effect on the mitochondrial membrane potential and also illustrates the induction of apoptosis along the mitochondrial pathway. An increase in ROS production leads to the mitochondrial dysfunction and, subsequently, to cell death. In this regard, the effect of compounds **4b**, **5b**, **6a** and **8** at $IC_{50}/2$ and IC_{50} concentrations on ROS production in HuTu 80 cells

Preprints (www.preprints.org) | NOT PEER-REVIEWED | Posted: 22 September 2023 doi:10.20944/preprints202309.1553.v1

was investigated using flow cytometry analysis and CellROX ® Deep Red flow cytometry kit. The data presented in Figure 10 show an increase in the fluorescence intensity of CellROX ® Deep Red after treatment with compounds **4b**, **5b**, **6a** and **8** at concentrations $IC_{50}/2$ and IC_{50} compared to the control (uncolored cells). It can be seen that HuTu 80 cells begin to produce ROS most actively in the presence of **4b** and **6a**. Compounds **5b** and **8** enhance the generation of ROS mainly in the concentration of IC_{50}.

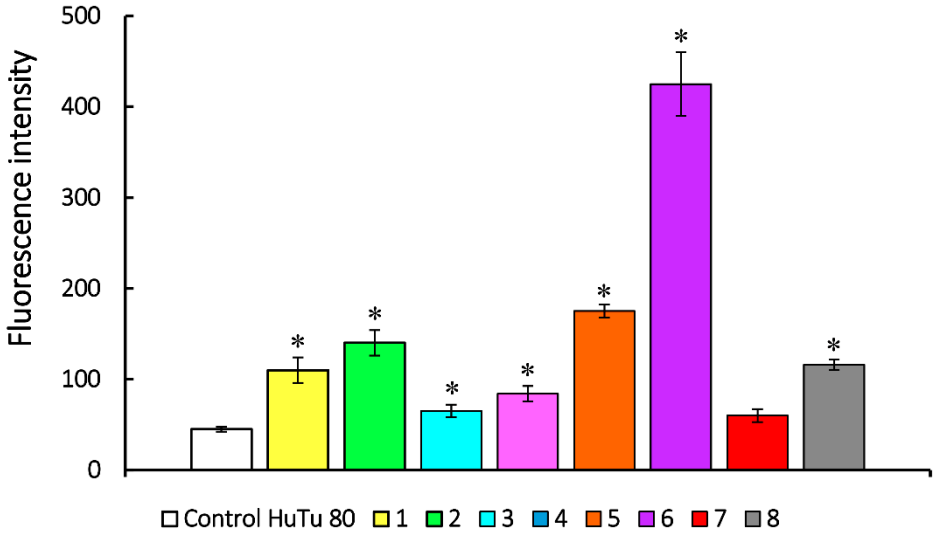

Figure 10. Induction of ROS production by compounds **4b**, **5b**, **6a** and **8** on HuTu 80 cell line; 1) **4b** – at concentration $IC_{50}/2$ (1.6 μM); 2) **4b** – at concentration IC_{50} (3.2 μM); 3) **5b** – at concentration $IC_{50}/2$ (2μM); 4) **5b** – at concentration IC_{50} (4 μM); 5) **6a** – at concentration $IC_{50}/2$ (0.05 μM); 6) **6a** – at concentration IC_{50} (0.1 μM); 7) **8** – at concentration $IC_{50}/2$ (0.045 μM); 8) **8** – at concentration IC_{50} (0.09 μM). Data are presented as mean ±SD of three independent experiments. *Values indicate $\rho < 0.05$.

3.2.6. Measurements of Caspase-9 and Caspase-8 by ELISA

To confirm that apoptosis induced by compounds **4b**, **5b**, **6a** and **8** proceeds along the internal (mitochondrial) pathway, studies were conducted to determine the enzymatic activity of the early apoptosis key markers – caspase 9 and caspase 8 using ELISA kits. The kits are sandwich enzyme immunoassay for in vitro quantitative measurement of Caspase 8 and Caspase 9 in cell lysates, rat tissue homogenates, and other biological fluids. HuTu 80 cells not treated with the tested compounds were used as a control. We calculated the concentration of caspase 9 and caspase 8 in ng/ml in experimental and control samples. The results are shown in Figure 11. It can be seen that the concentration of caspase 9, which plays a key role in the mitochondrial signaling pathway of apoptosis induction, in samples treated with compounds **4b**, **5b**, **6a** and **8** at concentrations of $IC_{50}/2$ and IC_{50} (Figure 11A) significantly increases compared to the control. The lowest concentration of caspase 9 is shown for compound **6a**, which is consistent with the data on the assessment of apoptosis by flow cytometry (Figure 8). The concentration of caspase 8, the activation of which characterizes the external (receptor-dependent pathway of apoptosis), significantly decreases relative to the control after treatment with substances **4b** and **5b**. At the same time, in the case of **6a** and **8**, it changes slightly compared to the control values (Figure 11B). Thus, it can be assumed that the studied compounds have a cytotoxic effect due to the induction of apoptosis proceeding along the mitochondrial pathway.

Preprints (www.preprints.org) | NOT PEER-REVIEWED | Posted: 22 September 2023 doi:10.20944/preprints202309.1553.v1

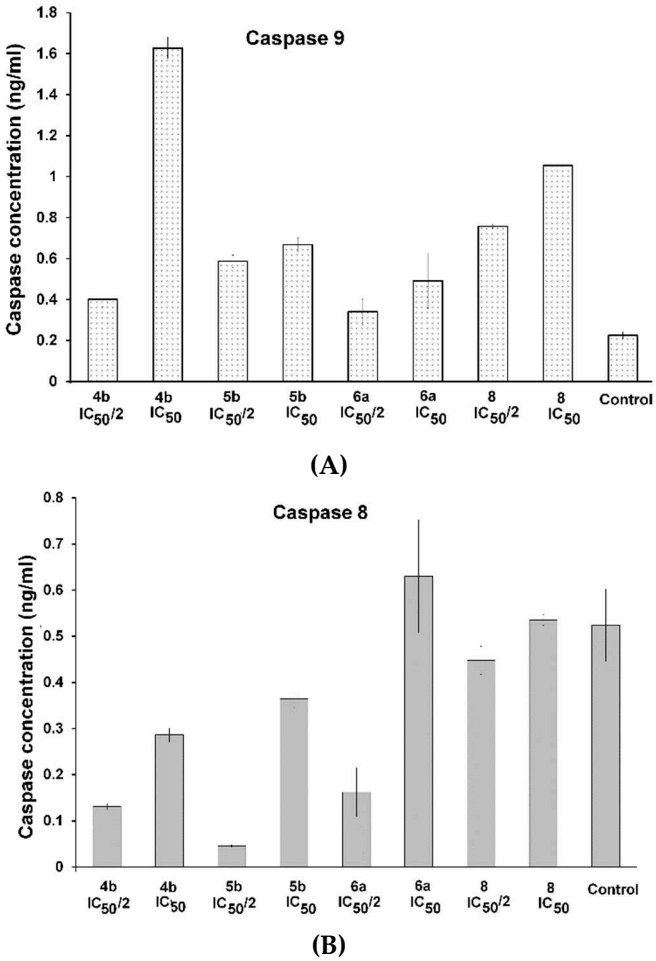

Figure 11. Quantitative measurement of caspase in cell lysates HuTu 80 *in vitro*. (**a**) – measurement of caspase 9 after treatment at **4b**, **5b**, **6a** and **8** in concentrations $IC_{50}/2$ и IC_{50}; (**b**) – measurement of caspase 8 after treatment at **4b**, **5b**, **6a** and **8** in concentrations $IC_{50}/2$ и IC_{50}; Data are presented as mean ±SD of three independent experiments. *Values indicate $\rho < 0.05$.

3.2.7. Effect of Aminophosphonium salts on cell cycle in cancer cells

The drugs that induce ROS and mitochondrial apoptosis in cancer cells cause disruption of cell cycle phases and proliferation [102,103]. Therefore, the effect of **4b**, **5b**, **6a** and **8** on the passage of HuTu 80 cells through the cell cycle was investigated using the classical fluorescent method, which allows determining at which phase the cell cycle was stopped. The studies were carried out using a fluorescent dye propidium iodide, which binds in proportion to the amount of DNA present in the cell. The diagram in Figure 12 shows the number of cells in each phase of the cell cycle. Analysis of the HuTu 80 cell cycle after treatment with compounds at IC_{50} concentrations for 48 hours revealed a significant delay of cells in the G0/G1 phase for **4b**, **5b** and **8** compared with the control. Compound **6a** caused a slight change in the cell cycle.

Preprints (www.preprints.org) | NOT PEER-REVIEWED | Posted: 22 September 2023 doi:10.20944/preprints202309.1553.v1

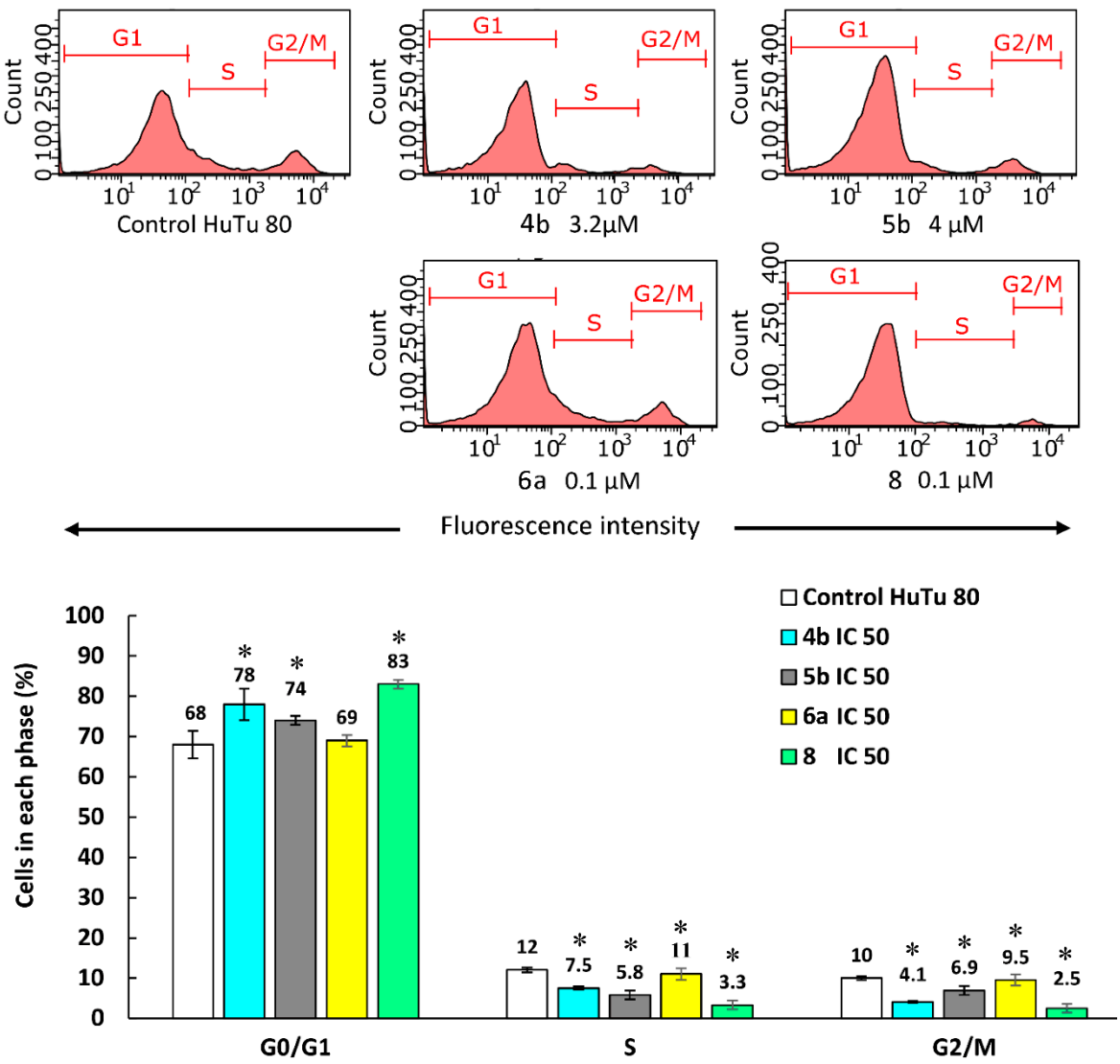

Figure 12. Effect of compounds **4b**, **5b**, **6a** and **8** at concentrations IC_{50} in HuTu 80 cells. Percentage of cells in the G0/G1, S, and G2/M phases (data are presented as mean ±SD of three independent experiments). *Values indicate $\rho < 0.05$.

3.2.8. Antibacterial Activity of Aminophosphonium Salts

Drugs with both antitumor and antimicrobial effects are currently actively used for malignant tumors of various origins [104]. In this regard, we studied the antibacterial and antifungal activity of the obtained compounds, including against resistant strains of microorganisms that pose a serious threat to human health around the world.

The synthesized compounds were tested for antibacterial (bacteriostatic and bactericidal) activity against a number of gram-positive *S. aureus 209P (Sa)*, *B. cereus* 8035 *(Bc)* and gram-negative bacteria *E. coli F-50 (Ec)*, *Pseudomonas aeruginosa 9027 (Pa)*, including against methicillin-resistant strains of *S. aureus (MRSA-1, MRSA-2)*. Antifungal activity was studied on a culture of the yeast-like fungus *Candida albican*s 10231. The data are presented in Table 4.

Preprints (www.preprints.org) | NOT PEER-REVIEWED | Posted: 22 September 2023 doi:10.20944/preprints202309.1553.v1

Table 4. Antimicrobial activity of aminophosphonium salts **4-6**.

Compounds	Minimum inhibitory concentration (MIC), μM							
	Gram-positive bacteria					Gram-negative bacteria		Yeast
	Sa	*Bc*	*Ef*	*MRSA-1*	*MRSA-2*	*Ec*	*Pa*	*Ca*
4a	62.5±5.2	62.5±5.3	250±21	125±10	125±11	–	–	–
4b	15.6±1.3	7.8±0.7	250±19	15.6±0.3	15.6±1.2	–	–	–
4c	3.9±0.3	3.9±0.3	62.5±5.2	3.9±0.4	7.8±0.6	500±48	–	–
4d	1.9±0.1	0.9±0.07	15.6±1.3	0.9±0.07	1.9±0.1	125±9	500±47	125±11
4e	0.25±0.01	0.5±0.04	0.5±0.04	0.5±0.04	0.25±0.02	15.6±1.3	7.8±0.6	1.9±0.1
9	34.3±5.4	274±48	-	137±19	34.3±5.3	–	–	–
5b	7.8±0.6	7.8±0.6	125±11	15.6±1.2	15.6±1.2	–	500±46	–
5c	3.9±0.3	3.9±0.3	31.3±2.2	3.9±0.3	3.9±0.4	250±19	–	–
5d	0.9±0.07	0.9±0.08	15.6±1.2	0.9±0.08	0.9±0.08	62.5±5.4	500±48	250±21
6a	62.5±5.5	31.3±2.3	125±11	62.5±5.3	62.5±5.6	–	–	–
6b	7.8±0.6	3.9±0.4	62.5±5.5	7.8±0.6	7.8±0.6	–	–	–
6c	3.9±0.3	1.9±0.1	31.3±5.4	3.9±0.3	3.9±0.4	500±46	250±21	500±47
6d	0.9±0.08	0.9±0.08	3.9±0.3	0.5±0.03	0.5±0.03	62.5±5.3	125±10	62.5±5.4
6e	0.5±0.04	0.9±0.08	0.5±0.03	0.5±0.04	0.5±0.03	31.3±2.4	3.9±0.3	1.9±0.1
8	0.9±0.07	0.9±0.07	15.6±1.2	1.9±0.1	3.9±0.3	500±47	–	–
7	250±20	500±47	–	250±19	250±20	–	–	–
Norfloxacin	7.5±0.5	24.4±2.1	24.4±2.2	–	7.5±0.5	4.7±0.02	12.1±1.1	–
Ketoconazole	–	–	–	–	–	–	–	7.3±0.5
Minimum bactericidal and fungicidal concentrations (MBC, MFC), μM								
4a	250±20	–	500±46	–	125±10	–	–	–
4b	31.3±2.3	–	–	500±47	125±9	–	–	–
4c	250±18	>500	500±48	125±10	250±20	500±48	–	–
4d	31.3±2.5	250±22	>500	62.5±5.4	250±18	250±19	500±48	250±18
4e	0.9±0.07	7.8±0.6	1.9±0.1	0.5±0.04	0.25±0.02	62.5±5.2	7.8±0.6	7.8±0.6
9	137±21	–	–	137±18	137±21	–	–	–
5b	250±20	–	–	500±48	250±20	500±49	–	–
5c	125±10	500±48	500±48	62.5±5.5	62.5±5.4	500±48	>500	–
5d	125±9	500±47	125±9	125±11	62.5±5.2	62.5±5.3	500±47	–
6a	125±10	500±46	–	500±47	62.5±5.6	–	–	–
6b	125±11	–	–	31.3±2.6	31.3±2.5	–	–	–
6c	125±11	>500	–	62.5±5.4	7.8±0.7	500±47	250±21	–
6d	62.5±5.4	250±21	250±19	0.9±0.07	0.9±0.08	62.5±5.5	125±9	250±19
6e	0.5±0.04	31.3±2.5	0.9±0.1	1.9±0.1	0.5±0.04	125±11	3.9±0.4	15.6±1.2
8	62.5±5.3	500±47	–	15.6±1.2	15.6±1.3	–	–	–
7	–	–	–	–	500±47	–	–	–
Norfloxacin	7.5±0.6	24.4±2.1	24.4±1.9	–	7.5±0.6	24.4±2.3	49.0±4.2	
Ketoconazole								7.3±0.5

Average of three values measured; ± standard deviation (SD); - means non-active.

The tested compounds showed selective activity against all gram-positive bacteria, including MRSA strains. Most Aminophosphonium salts showed antimicrobial action at the level of the fluoroquinolone antibiotic norfloxacin, and in some cases even significantly exceeded the activity of this comparison drug. Of particular note is substance **4e**, which showed the highest antimicrobial activity against all gram-positive and gram-negative bacteria and against *Candida albicans 10231*. Moreover, it acted bactericidal and fungicidal, i.e., MIC and MBC (MBC) differ from each other by no more than 4 times.

Preprints (www.preprints.org) | NOT PEER-REVIEWED | Posted: 22 September 2023 doi:10.20944/preprints202309.1553.v1

3.2.9. Hemolytic action of test compounds

The hemolytic activity of chemical compounds can be used as a means of their toxicological assessment. In this regard, a concentration (HC_{50}) was determined for compounds **4b**, **5b** and **6a**, causing hemolysis of 50% of erythrocytes. Data on the hemolytic activity of compounds **4b**, **5b** and **6a** are given in Table. 5. It can be seen that the HC_{50} values of these compounds are > 100 μM. Gramicidin C was used as a comparison drug. The results indicate the high selectivity of the tested compounds with respect to bacterial cells and low toxicity with respect to the human blood cells and may be of interest for further studies on living objects.

Table 5. Hemolytic activity of Aminophosphonium salts*.

Test compound	HC_{50} (μM)
4b	> 100
5b	> 100
6b	> 100
Gramicidin S	9.4 ± 0.8

* – The experiments were repeated for three times. The results are expressed as the mean ± standard deviation (SD).

3.2.10. In vivo Study of Acute Toxicity of Aminophosphonic Salts

The study of the acute toxicity parameters of six aminophosphonium salts **4a**, **4b**, **4d**, **5a**, **5b** and **6b** was performed on male outbreed white mice of the CD-1 line. Acute toxicity was determined with a single parenteral – intraperitoneal (intraperitoneal) administration in the form of solutions in 40% DMSO at doses from 1 to 1000 mg / kg. To assess acute toxicity, the animals were monitored 14 days after the introduction of substances, assessing their general condition and recording deaths. Next, lethal doses of LD_{50}, LD_0, LD_{16}, LD_{84}, and LD_{100} substances were calculated using the Probit analysis method. The results of the calculation of LD_{50} are given in Table 6, the data LD_0, LD_{16}, LD_{84}, LD_{100} are given in Supplemental (Table S1).

Table 6. Acute toxicity of compounds **4a**, **4b**, **4d**, **5a**, **5b** and **6b.**

Compound	LD_{50}, mg/kg
4a	37.5
4b	48.7
4d	6.9
5a	37.5
5b	25.0
6b	106.5

In the control group of animals that were injected with a solvent – 40% DMSO on saline solution in an amount of 0.1 ml/10 g (10 ml/kg), there was no death or signs of depression of the animals. It is shown that among the studied substances, **4d** (LD_{50} 6.9 mg/kg) has the highest toxicity, which, according to the classification [105], belongs to the class of highly toxic compounds. Substances **4a**, **4b**, **5a**, **5b** and **6b** in the range from 37.5 to 106.5 mg/kg can be classified as moderately toxic compounds. It should be noted the similarity in the manifestation of the toxic effect for substances **4a**, **4b**, **4d**, **5a** and **5b**, namely, the rapid onset of death of the animal within 1-2 hours after administration in doses of LD_{100}. With the introduction of substance **6b** at a dose of 150 mg / kg, which causes 100% death of animals, deaths were observed a day after administration. With the introduction of substance **6b** in higher doses of 200 and 400 mg / kg, death occurred within 10 minutes after administration. Under the influence of substances in lower doses ($LD_{16\text{-}50}$), deaths of animals were observed after 1-12 days. Among the symptoms, convulsions, rapid heartbeat, heavy breathing were observed, which probably indicates an effect on the central nervous system.

4. Conclusions

In this work, the synthesis of various amphiphilic phosphonium salts containing a diethylamino-groups was carried out by the interaction of hexaethyltriaminophosphine **1**, bis(tetraethyldiamino)phenylphosphine **2** and diethylaminodiphenylphosphine **3** with alkyl iodides and tetradecyl bromide under mild conditions in acetonitrile. The structure of obtained salts is proved by NMR and also by XRD for (diethylamino)(octyl)diphenylphosphonium iodide **6a**. In vitro cytotoxicity and in vivo toxicity were evaluated. Nanotherapeutic forms based on lipids (liposomes and solid lipid nanoparticles) and amphiphilic phosphonium salts were developed. The zeta potential of lipid nanosystems decorated by amphiphilic aminophosphonic compounds moves to positive values. An increase the size (from 100 to 150 nm) and polydispersity index (from 0.24 to 0.47) for solid lipid nanoparticles are found. The internalization of dyes-labeled liposomes and solid lipid nanoparticles by tumor cells within 1 hour are shown by flow cytometry. Most of compounds exhibit a high cytotoxicity towards to the M-Hela cell lines: IC_{50} is in the range of 0.24-1.8 μM with selectivity index (SI) 1.6-17. The highest SI was fond for **4d** (SI 7.1), **6a** (SI 4.8) and **6b** (SI 17). Among them **6b** is a leader with two times lower IC_{50} than for reference drug doxorubicin. A pronounced dependence of increasing SI on the nature of aminophosphonium cation is observed **4** < **5** < **6** at a rather low IC_{50} 0.06-4.0 μM for **4**-**6** on the HuTu 80 cell lines. The highest SI is observed for **4e** (SI 28), **5a** (SI 210), **6a** (SI 277). A similar behavior was fond for PC3, Du-145 and PANC-1 cell lines, where monoaminophosphonium compounds are the most effective with IC_{50} (SI) values in the range 0.3-5.5 μM (6.4-20). Monoaminophosphonium derivatives **6** are more cytotoxic with higher SI compared to tri- and diaminophosphonium salts **4** and **5**. Cytotoxicity increases with the length of R substituent at the phosphorus atom on the HuTu 80, PC3 and Du-145 cell lines. The lipid systems with aminophosphonium salts provides an improvement of the cytotoxic activity against tumor cells compared to their individual compounds and a decrease the toxicity against normal cell lines. The IC_{50} of PC/**4c**, PC/**4d**, PC/**5b**, PC/**5c**, PC/**5d** and SLN/**4b** lipid systems are lower than for reference drug DOX with high SI = 53 and 56 and SI = 30 for the SLN/**4b** and PC/**4c** toward to MCF-7 and DU-145. The mechanism of cytotoxicity of **4b**, **5b**, **6a** and **8** appears to involve the intrinsic mitochondrial apoptotic pathway. This is also consistent with the data on the production of ROS and the enzymatic activity of early apoptosis key markers – caspase 9 and caspase 8 as well as the effect on the phases of cell cycle and proliferation. Synthesized aminophosphonium salts exhibit a high selective activity against Gram-positive bacteria *S. aureus 209P*, *B. segeus 8035*, including methicillin-resistant strains of *S. aureus (MRSA-1, MRSA-2)*, comparable to the reference fluoroquinolone antibiotic norfloxacin. A leader tetradecyl-tris(diethylamino)phosphonium bromide **4e** shows the highest antimicrobial activity against all studied gram-positive and gram-negative bacteria, as well as against *Candida albicans 10231* fungi. **4b**, **5b** and **6a** with a high cytotoxicity, demonstrated their low toxicity to the human blood cells. A moderate in vivo toxicity in CD-1 mice was established for the lead compounds. This indicates the interest for further research on living objects.

Supplementary Materials: The following supporting information can be downloaded at the website of this paper posted on Preprints.org., Figures S1-S165: NMR spectra of synthesized compounds **4**-**9**; Table S1: Acute toxicity parameters $LD_{0\text{-}100}$ of compounds **4a**, **4b**, **4d**, **5a**, **5b**, **6b**. Information on X-ray diffraction analysis (cif and checkcif files) of compound **6a** is also available.

Author Contributions: All authors contributed to the writing of the manuscript and all authors approved the final version of the manuscript. Investigation, M.N.D., A.D.V., A.B.V., I.A.L., A.P.L., A.S.S., D.F.A. and V.V.Z.; Supervision, V.F.M.; Writing – original draft, O.V.Ts.; Writing – review & editing, A.V.N. and T.N.P.

Funding: This research was funded by the Ministry of Science and Higher Education of the Russian Federation, Agreement number 075-15-2020-777.

Data Availability Statement: The data presented in this study are available on request from the corresponding author.

Acknowledgments: The financial support by the Ministry of Science and Higher Education of the Russian Federation (Agreement No. 075-15-2020-777) is gratefully acknowledged. The measurements have been carried out using the equipment of Distributed Spectral-Analytical Center of Shared Facilities for Study of Structure,

Composition and Properties of Substances and Materials of FRC Kazan Scientific Center of RAS and Interdisciplinary Centre for Shared Use of Kazan Federal University.

Conflicts of Interest: The authors declare no conflict of interest.

References

1. Pourahmad, J.; Salimi, A.; Seydi, E. Mitochondrial Targeting for Drug Development. In *Toxicology Studies - Cells, Drugs and Environment*; InTech, 2015.
2. Cojocaru, K.-A.; Luchian, I.; Goriuc, A.; Antoci, L.-M.; Ciobanu, C.-G.; Popescu, R.; Vlad, C.-E.; Blaj, M.; Foia, L.G. Mitochondrial Dysfunction, Oxidative Stress, and Therapeutic Strategies in Diabetes, Obesity, and Cardiovascular Disease. *Antioxidants* **2023**, *12*, 658, doi:10.3390/antiox12030658.
3. Alqahtani, T.; Deore, S.L.; Kide, A.A.; Shende, B.A.; Sharma, R.; Dadarao Chakole, R.; Nemade, L.S.; Kishor Kale, N.; Borah, S.; Shrikant Deokar, S.; et al. Mitochondrial dysfunction and oxidative stress in Alzheimer's disease, and Parkinson's disease, Huntington's disease and Amyotrophic Lateral Sclerosis -An updated review. *Mitochondrion* **2023**, *71*, 83–92, doi:10.1016/j.mito.2023.05.007.
4. Danieli, M.G.; Antonelli, E.; Piga, M.A.; Cozzi, M.F.; Allegra, A.; Gangemi, S. Oxidative stress, mitochondrial dysfunction, and respiratory chain enzyme defects in inflammatory myopathies. *Autoimmun. Rev.* **2023**, *22*, 103308, doi:10.1016/j.autrev.2023.103308.
5. Behl, T.; Makkar, R.; Anwer, M.K.; Hassani, R.; Khuwaja, G.; Khalid, A.; Mohan, S.; Alhazmi, H.A.; Sachdeva, M.; Rachamalla, M. Mitochondrial Dysfunction: A Cellular and Molecular Hub in Pathology of Metabolic Diseases and Infection. *J. Clin. Med.* **2023**, *12*, 2882, doi:10.3390/jcm12082882.
6. Amorim, J.A.; Coppotelli, G.; Rolo, A.P.; Palmeira, C.M.; Ross, J.M.; Sinclair, D.A. Mitochondrial and metabolic dysfunction in ageing and age-related diseases. *Nat. Rev. Endocrinol.* **2022**, *18*, 243–258, doi:10.1038/s41574-021-00626-7.
7. Liu, Y.; Sun, Y.; Guo, Y.; Shi, X.; Chen, X.; Feng, W.; Wu, L.-L.; Zhang, J.; Yu, S.; Wang, Y.; et al. An Overview: The Diversified Role of Mitochondria in Cancer Metabolism. *Int. J. Biol. Sci.* **2023**, *19*, 897–915, doi:10.7150/ijbs.81609.
8. Martini, H.; Passos, J.F. Cellular senescence: all roads lead to mitochondria. *FEBS J.* **2023**, *290*, 1186–1202, doi:10.1111/febs.16361.
9. Grasso, D.; Zampieri, L.X.; Capelôa, T.; Van de Velde, J.A.; Sonveaux, P. Mitochondria in cancer. *Cell Stress* **2020**, *4*, 114–146, doi:10.15698/cst2020.06.221.
10. Nath, S.; Villadsen, J. Oxidative phosphorylation revisited. *Biotechnol. Bioeng.* **2015**, *112*, 429–437, doi:10.1002/bit.25492.
11. Shi, L.; Tu, B.P. Acetyl-CoA and the regulation of metabolism: mechanisms and consequences. *Curr. Opin. Cell Biol.* **2015**, *33*, 125–131, doi:10.1016/j.ceb.2015.02.003.
12. Obi, C.D.; Bhuiyan, T.; Dailey, H.A.; Medlock, A.E. Ferrochelatase: Mapping the Intersection of Iron and Porphyrin Metabolism in the Mitochondria. *Front. Cell Dev. Biol.* **2022**, *10*, doi:10.3389/fcell.2022.894591.
13. Melchinger, P.; Garcia, B.M. Mitochondria are midfield players in steroid synthesis. *Int. J. Biochem. Cell Biol.* **2023**, *160*, 106431, doi:10.1016/j.biocel.2023.106431.
14. Moldogazieva, N.T.; Mokhosoev, I.M.; Feldman, N.B.; Lutsenko, S. V. ROS and RNS signalling: adaptive redox switches through oxidative/nitrosative protein modifications. *Free Radic. Res.* **2018**, *52*, 507–543, doi:10.1080/10715762.2018.1457217.
15. Di Meo, S.; Reed, T.T.; Venditti, P.; Victor, V.M. Role of ROS and RNS Sources in Physiological and Pathological Conditions. *Oxid. Med. Cell. Longev.* **2016**, *2016*, 1–44, doi:10.1155/2016/1245049.
16. Haskins, N.; Bhuvanendran, S.; Anselmi, C.; Gams, A.; Kanholm, T.; Kocher, K.M.; LoTempio, J.; Krohmaly, K.I.; Sohai, D.; Stearrett, N.; et al. Mitochondrial Enzymes of the Urea Cycle Cluster at the Inner Mitochondrial Membrane. *Front. Physiol.* **2021**, *11*, doi:10.3389/fphys.2020.542950.
17. Matuz-Mares, D.; González-Andrade, M.; Araiza-Villanueva, M.G.; Vilchis-Landeros, M.M.; Vázquez-Meza, H. Mitochondrial Calcium: Effects of Its Imbalance in Disease. *Antioxidants* **2022**, *11*, 801, doi:10.3390/antiox11050801.
18. Green, D.R. The Mitochondrial Pathway of Apoptosis. *Cold Spring Harb. Perspect. Biol.* **2022**, *14*, a041038, doi:10.1101/cshperspect.a041038.
19. Green, D.R. The Mitochondrial Pathway of Apoptosis Part II: The BCL-2 Protein Family. *Cold Spring Harb. Perspect. Biol.* **2022**, *14*, a041046, doi:10.1101/cshperspect.a041046.
20. Zhou, Q.; Tao, C.; Yuan, J.; Pan, F.; Wang, R. Ferroptosis, a subtle talk between immune system and cancer cells: To be or not to be? *Biomed. Pharmacother.* **2023**, *165*, 115251, doi:10.1016/j.biopha.2023.115251.
21. Liu, Y.; Lu, S.; Wu, L.; Yang, L.; Yang, L.; Wang, J. The diversified role of mitochondria in ferroptosis in cancer. *Cell Death Dis.* **2023**, *14*, 519, doi:10.1038/s41419-023-06045-y.
22. Wang, H.; Liu, C.; Zhao, Y.; Gao, G. Mitochondria regulation in ferroptosis. *Eur. J. Cell Biol.* **2020**, *99*, 151058, doi:10.1016/j.ejcb.2019.151058.

23. Baines, C.P. Role of the Mitochondrion in Programmed Necrosis. *Front. Physiol.* **2010**, *1*, doi:10.3389/fphys.2010.00156.
24. Faizan, M.I.; Ahmad, T. Altered mitochondrial calcium handling and cell death by necroptosis: An emerging paradigm. *Mitochondrion* **2021**, *57*, 47–62, doi:10.1016/j.mito.2020.12.004.
25. Yousif, L.F.; Stewart, K.M.; Kelley, S.O. Targeting Mitochondria with Organelle-Specific Compounds: Strategies and Applications. *ChemBioChem* **2009**, *10*, 1939–1950, doi:10.1002/cbic.200900185.
26. Madak, J.; Neamati, N. Membrane Permeable Lipophilic Cations as Mitochondrial Directing Groups. *Curr. Top. Med. Chem.* **2015**, *15*, 745–766, doi:10.2174/1568026615666150302105622.
27. Zielonka, J.; Joseph, J.; Sikora, A.; Hardy, M.; Ouari, O.; Vasquez-Vivar, J.; Cheng, G.; Lopez, M.; Kalyanaraman, B. Mitochondria-Targeted Triphenylphosphonium-Based Compounds: Syntheses, Mechanisms of Action, and Therapeutic and Diagnostic Applications. *Chem. Rev.* **2017**, *117*, 10043–10120, doi:10.1021/acs.chemrev.7b00042.
28. Pawar, A.; Korake, S.; Pawar, A.; Kamble, R. Delocalized Lipophilic Cation Triphenyl Phosphonium: Promising Molecule for Mitochondria Targeting. *Curr. Drug Deliv.* **2023**, *20*, 1217–1223, doi:10.2174/1567201819666220525092527.
29. Begum, H.M.; Shen, K. Intracellular and microenvironmental regulation of mitochondrial membrane potential in cancer cells. *WIREs Mech. Dis.* **2023**, *15*, doi:10.1002/wsbm.1595.
30. Potter, M.; Newport, E.; Morten, K.J. The Warburg effect: 80 years on. *Biochem. Soc. Trans.* **2016**, *44*, 1499–1505, doi:10.1042/BST20160094.
31. Wang, Y.; Patti, G.J. The Warburg effect: a signature of mitochondrial overload. *Trends Cell Biol.* **2023**, doi:10.1016/j.tcb.2023.03.013.
32. Cheng, X.; Feng, D.; Lv, J.; Cui, X.; Wang, Y.; Wang, Q.; Zhang, L. Application Prospects of Triphenylphosphine-Based Mitochondria-Targeted Cancer Therapy. *Cancers (Basel).* **2023**, *15*, 666, doi:10.3390/cancers15030666.
33. Zaib, S.; Hayyat, A.; Ali, N.; Gul, A.; Naveed, M.; Khan, I. Role of Mitochondrial Membrane Potential and Lactate Dehydrogenase A in Apoptosis. *Anticancer. Agents Med. Chem.* **2022**, *22*, 2048–2062, doi:10.2174/1871520621666211126090906.
34. Khailova, L.S.; Nazarov, P.A.; Sumbatyan, N. V.; Korshunova, G.A.; Rokitskaya, T.I.; Dedukhova, V.I.; Antonenko, Y.N.; Skulachev, V.P. Uncoupling and toxic action of alkyltriphenylphosphonium cations on mitochondria and the bacterium Bacillus subtilis as a function of alkyl chain length. *Biochem.* **2015**, *80*, 1589–1597, doi:10.1134/S000629791512007X.
35. Tellería, F.; Mansilla, S.; Méndez, D.; Sepúlveda, M.; Araya-Maturana, R.; Castro, L.; Trostchansky, A.; Fuentes, E. The Use of Triphenyl Phosphonium Cation Enhances the Mitochondrial Antiplatelet Effect of the Compound Magnolol. *Pharmaceuticals* **2023**, *16*, 210, doi:10.3390/ph16020210.
36. Montecino-Garrido, H.; Sepúlveda, M.; Méndez, D.; Monroy-Cárdenas, M.; Alfaro, S.; González-Avendaño, M.; Caballero, J.; Urra, F.A.; Araya-Maturana, R.; Fuentes, E. Assessing mitochondria-targeted acyl hydroquinones on the mitochondrial platelet function and cytotoxic activity: Role of the linker length. *Free Radic. Biol. Med.* **2023**, *208*, 26–36, doi:10.1016/j.freeradbiomed.2023.07.030.
37. Uno, S.; Harkiss, A.H.; Chowdhury, R.; Caldwell, S.T.; Prime, T.A.; James, A.M.; Gallagher, B.; Prudent, J.; Hartley, R.C.; Murphy, M.P. Incorporating a Polyethyleneglycol Linker to Enhance the Hydrophilicity of Mitochondria-Targeted Triphenylphosphonium Constructs. *ChemBioChem* **2023**, *24*, doi:10.1002/cbic.202200774.
38. Yang, S.; Yoon, N.G.; Park, M.-A.; Yun, J.; Im, J.Y.; Kang, B.H.; Kang, S. Triphenylphosphonium conjugation to a TRAP1 inhibitor, 2-amino-6-chloro-7,9-dihydro-8H-purin-8-one increases antiproliferative activity. *Bioorg. Chem.* **2022**, *126*, 105856, doi:10.1016/j.bioorg.2022.105856.
39. Tsepaeva, O. V.; Salikhova, T.I.; Grigor'eva, L.R.; Ponomaryov, D. V.; Dang, T.; Ishkaeva, R.A.; Abdullin, T.I.; Nemtarev, A. V.; Mironov, V.F. Synthesis and in vitro evaluation of triphenylphosphonium derivatives of acetylsalicylic and salicylic acids: structure-dependent interactions with cancer cells, bacteria, and mitochondria. *Med. Chem. Res.* **2021**, *30*, 925–939, doi:10.1007/s00044-020-02674-6.
40. Ong, H.C.; Coimbra, J.T.S.; Kwek, G.; Ramos, M.J.; Xing, B.; Fernandes, P.A.; García, F. Alkyl vs. aryl modifications: a comparative study on modular modifications of triphenylphosphonium mitochondrial vectors. *RSC Chem. Biol.* **2021**, *2*, 1643–1650, doi:10.1039/D1CB00099C.
41. Strobykina, I.Yu.; Voloshina, A.D.; Andreeva, O. V.; Sapunova, A.S.; Lyubina, A.P.; Amerhanova, S.K.; Belenok, M.G.; Saifina, L.F.; Semenov, V.E.; Kataev, V.E. Synthesis, antimicrobial activity and cytotoxicity of triphenylphosphonium (TPP) conjugates of 1,2,3-triazolyl nucleoside analogues. *Bioorg. Chem.* **2021**, *116*, 105328, doi:10.1016/j.bioorg.2021.105328.
42. Millard, M.; Pathania, D.; Shabaik, Y.; Taheri, L.; Deng, J.; Neamati, N. Preclinical Evaluation of Novel Triphenylphosphonium Salts with Broad-Spectrum Activity. *PLoS One* **2010**, *5*, e13131, doi:10.1371/journal.pone.0013131.

43. Trnka, J.; Elkalaf, M.; Anděl, M. Lipophilic Triphenylphosphonium Cations Inhibit Mitochondrial Electron Transport Chain and Induce Mitochondrial Proton Leak. *PLoS One* **2015**, *10*, e0121837, doi:10.1371/journal.pone.0121837.
44. Gardner, Z.S.; Schumacher, T.J.; Ronayne, C.T.; Kumpati, G.P.; Williams, M.J.; Yoshimura, A.; Palle, H.; Mani, C.; Rumbley, J.; Mereddy, V.R. Synthesis and biological evaluation of novel 2-alkoxycarbonylallylester phosphonium derivatives as potential anticancer agents. *Bioorg. Med. Chem. Lett.* **2021**, *45*, 128136, doi:10.1016/j.bmcl.2021.128136.
45. Kulkarni, C.A.; Fink, B.D.; Gibbs, B.E.; Chheda, P.R.; Wu, M.; Sivitz, W.I.; Kerns, R.J. A Novel Triphenylphosphonium Carrier to Target Mitochondria without Uncoupling Oxidative Phosphorylation. *J. Med. Chem.* **2021**, *64*, 662–676, doi:10.1021/acs.jmedchem.0c01671.
46. AbuEid, M.; Keyes, R.F.; McAllister, D.; Peterson, F.; Kadamberi, I.P.; Sprague, D.J.; Chaluvally-Raghavan, P.; Smith, B.C.; Dwinell, M.B. Fluorinated triphenylphosphonium analogs improve cell selectivity and in vivo detection of mito-metformin. *iScience* **2022**, *25*, 105670, doi:10.1016/j.isci.2022.105670.
47. Rokitskaya, T.I.; Kotova, E.A.; Luzhkov, V.B.; Kirsanov, R.S.; Aleksandrova, E. V.; Korshunova, G.A.; Tashlitsky, V.N.; Antonenko, Y.N. Lipophilic ion aromaticity is not important for permeability across lipid membranes. *Biochim. Biophys. Acta - Biomembr.* **2021**, *1863*, 183483, doi:10.1016/j.bbamem.2020.183483.
48. Rokitskaya, T.I.; Aleksandrova, E. V.; Korshunova, G.A.; Khailova, L.S.; Tashlitsky, V.N.; Luzhkov, V.B.; Antonenko, Y.N. Membrane Permeability of Modified Butyltriphenylphosphonium Cations. *J. Phys. Chem. B* **2022**, *126*, 412–422, doi:10.1021/acs.jpcb.1c08135.
49. Rokitskaya, T.I.; Luzhkov, V.B.; Korshunova, G.A.; Tashlitsky, V.N.; Antonenko, Y.N. Effect of methyl and halogen substituents on the transmembrane movement of lipophilic ions. *Phys. Chem. Chem. Phys.* **2019**, *21*, 23355–23363, doi:10.1039/C9CP03460A.
50. Milane, L.; Dolare, S.; Jahan, T.; Amiji, M. Mitochondrial nanomedicine: Subcellular organelle-specific delivery of molecular medicines. *Nanomedicine Nanotechnology, Biol. Med.* **2021**, *37*, 102422, doi:10.1016/j.nano.2021.102422.
51. Liew, S.S.; Qin, X.; Zhou, J.; Li, L.; Huang, W.; Yao, S.Q. Smart Design of Nanomaterials for Mitochondria-Targeted Nanotherapeutics. *Angew. Chemie Int. Ed.* **2021**, *60*, 2232–2256, doi:10.1002/anie.201915826.
52. Allemailem, K.S.; Almatroudi, A.; Alsahli, M.A.; Aljaghwani, A.; M El-Kady, A.; Rahmani, A.H.; Khan, A.A. Novel Strategies for Disrupting Cancer-Cell Functions with Mitochondria-Targeted Antitumor Drug–Loaded Nanoformulations. *Int. J. Nanomedicine* **2021**, *Volume 16*, 3907–3936, doi:10.2147/IJN.S303832.
53. Yamada, Y.; Satrialdi; Hibino, M.; Sasaki, D.; Abe, J.; Harashima, H. Power of mitochondrial drug delivery systems to produce innovative nanomedicines. *Adv. Drug Deliv. Rev.* **2020**, *154–155*, 187–209, doi:10.1016/j.addr.2020.09.010.
54. Wang, C.; Li, F.; Zhang, T.; Yu, M.; Sun, Y. Recent advances in anti-multidrug resistance for nano-drug delivery system. *Drug Deliv.* **2022**, *29*, 1684–1697, doi:10.1080/10717544.2022.2079771.
55. Buchke, S.; Sharma, M.; Bora, A.; Relekar, M.; Bhanu, P.; Kumar, J. Mitochondria-Targeted, Nanoparticle-Based Drug-Delivery Systems: Therapeutics for Mitochondrial Disorders. *Life* **2022**, *12*, 657, doi:10.3390/life12050657.
56. Mitragotri, S.; Anderson, D.G.; Chen, X.; Chow, E.K.; Ho, D.; Kabanov, A. V.; Karp, J.M.; Kataoka, K.; Mirkin, C.A.; Petrosko, S.H.; et al. Accelerating the Translation of Nanomaterials in Biomedicine. *ACS Nano* **2015**, *9*, 6644–6654, doi:10.1021/acsnano.5b03569.
57. Azarnezhad, A.; Samadian, H.; Jaymand, M.; Sobhani, M.; Ahmadi, A. Toxicological profile of lipid-based nanostructures: are they considered as completely safe nanocarriers? *Crit. Rev. Toxicol.* **2020**, *50*, 148–176, doi:10.1080/10408444.2020.1719974.
58. Hald Albertsen, C.; Kulkarni, J.A.; Witzigmann, D.; Lind, M.; Petersson, K.; Simonsen, J.B. The role of lipid components in lipid nanoparticles for vaccines and gene therapy. *Adv. Drug Deliv. Rev.* **2022**, *188*, 114416, doi:10.1016/j.addr.2022.114416.
59. Halwani, A.A. Development of Pharmaceutical Nanomedicines: From the Bench to the Market. *Pharmaceutics* **2022**, *14*, 106, doi:10.3390/pharmaceutics14010106.
60. German-Cortés, J.; Vilar-Hernández, M.; Rafael, D.; Abasolo, I.; Andrade, F. Solid Lipid Nanoparticles: Multitasking Nano-Carriers for Cancer Treatment. *Pharmaceutics* **2023**, *15*, 831, doi:10.3390/pharmaceutics15030831.
61. Moosavian, S.A.; Bianconi, V.; Pirro, M.; Sahebkar, A. Challenges and pitfalls in the development of liposomal delivery systems for cancer therapy. *Semin. Cancer Biol.* **2021**, *69*, 337–348, doi:10.1016/j.semcancer.2019.09.025.
62. Pashirova, T.N.; Nemtarev, A.V.; Souto, E.B.; Mironov, V.F. Triarylphosphonium compounds — effective vectors for mitochondrial-directed delivery systems: decoration strategies and prospects for clinical application. *Russ. Chem. Rev.* **2023**, *92*, doi:10.59761/RCR5095.
63. Mironov, V.F.; Nemtarev, A. V.; Tsepaeva, O. V.; Dimukhametov, M.N.; Litvinov, I.A.; Voloshina, A.D.; Pashirova, T.N.; Titov, E.A.; Lyubina, A.P.; Amerhanova, S.K.; et al. Rational Design 2-

Hydroxypropylphosphonium Salts as Cancer Cell Mitochondria-Targeted Vectors: Synthesis, Structure, and Biological Properties. *Molecules* **2021**, *26*, 6350, doi:10.3390/molecules26216350.
64. Tsepaeva, O. V.; Nemtarev, A. V.; Pashirova, T.N.; Khokhlachev, M. V.; Lyubina, A.P.; Amerkhanova, S.K.; Voloshina, A.D.; Mironov, V.F. Novel triphenylphosphonium amphiphilic conjugates of glycerolipid type: synthesis, cytotoxic and antibacterial activity, and targeted cancer cell delivery. *RSC Med. Chem.* **2023**, *14*, 454–469, doi:10.1039/D2MD00363E.
65. Grützmacher, H.; Marchand, C.M. Heteroatom stabilized carbenium ions. *Coord. Chem. Rev.* **1997**, *163*, 287–344, doi:10.1016/S0010-8545(97)00043-X.
66. Hudson, H.R.; Matthews, R.W.; McPartlin, M.; Pryce, M.A.; Shode, O.O. Quasiphosphonium intermediates. Part 7. The preparation of trinorborn-1-yl phosphite and its reactions with halogeno compounds: stable intermediates of the Arbuzov and Perkow reactions and their structural characterization by X-ray diffraction, NMR spectr. *J. Chem. Soc. Perkin Trans. 2* **1993**, 1433, doi:10.1039/p29930001433.
67. Nesterov, L. V.; Kessel, A.Y.; Mutalapova, R.I. Synthesis of Quasi-Phosphonium salts. *J. Gen. Chem. USSR (Engl. Transl.)* **1969**, *39*, 2394–2397.
68. Marchenko A.P.; Koidan, G.N.; Pinchuk, A.M. Reaction of tetrakis(dialkylamido)phosphonium bromides with bases. *J. Gen. Chem. USSR (Engl. Transl.)* **1984**, *54*, 2691–2696.
69. Schwesinger, R.; Schlemper, H.; Hasenfratz, C.; Willaredt, J.; Dambacher, T.; Breuer, T.; Ottaway, C.; Fletschinger, M.; Boele, J.; Fritz, H.; et al. Extremely Strong, Uncharged Auxiliary Bases; Monomeric and Polymer-Supported Polyaminophosphazenes (P 2 –P 5). *Liebigs Ann.* **1996**, 1055–1081, doi:10.1002/jlac.199619960705.
70. Kong, X.; Wadhwa, K.; Verkade, J.G.; Schmidt-Rohr, K. Determination of the Structure of a Novel Anion Exchange Fuel Cell Membrane by Solid-State Nuclear Magnetic Resonance Spectroscopy. *Macromolecules* **2009**, *42*, 1659–1664, doi:10.1021/ma802613k.
71. Stuebe, C.; Lankelma, H.P. Preparation of Some Hexaalkyl-phosphorous, Phosphoric and Phosphorothioic Triamides 1. *J. Am. Chem. Soc.* **1956**, *78*, 976–977, doi:10.1021/ja01586a027.
72. Ewart, G.; Payne, D.S.; Porte, A.L.; Lane, A.P. 783. Some aminophosphines. *J. Chem. Soc.* **1962**, 3984, doi:10.1039/jr9620003984.
73. Petrov, K.A.; Nifant'ev, E.E.; Lysenko, T.N.; Evdakov, V.P. Synthesis of esters of phosphorous and phosphonous acids by alcoholysis of their amides. *Zh. Obshch. Khim.* (*J. Gen. Chem. USSR)* **1961**, *31*, 2377–2380.
74. Kostag, M.; Liebert, T.; El Seoud, O.A.; Heinze, T. Efficient Cellulose Solvent: Quaternary Ammonium Chlorides. *Macromol. Rapid Commun.* **2013**, *34*, 1580–1584, doi:10.1002/marc.201300497.
75. Li, H.; Zhao, G.; Liu, F.; Zhang, S. Physicochemical Characterization of MF m – -Based Ammonium Ionic Liquids. *J. Chem. Eng. Data* **2013**, *58*, 1505–1515, doi:10.1021/je300993n.
76. APEX2 (Version 2.1), SAINTPlus, Data Reduction and Correction Program (Version 7.31A) Madison, Wisconsin, USA Bruker AXS Inc. 2006.
77. Sheldrick, G.M. SADABS, Version 2.10 2003.
78. Sheldrick, G.M. SHELXT – Integrated space-group and crystal-structure determination. *Acta Crystallogr. Sect. A Found. Adv.* **2015**, *71*, 3–8, doi:10.1107/S2053273314026370.
79. Sheldrick, G.M. Crystal structure refinement with SHELXL. *Acta Crystallogr. Sect. C Struct. Chem.* **2015**, *71*, 3–8, doi:10.1107/S2053229614024218.
80. Farrugia, L.J. WinGX and ORTEP for Windows : an update. *J. Appl. Crystallogr.* **2012**, *45*, 849–854, doi:10.1107/S0021889812029111.
81. Spek, A.L. Structure validation in chemical crystallography. *Acta Crystallogr. Sect. D Biol. Crystallogr.* **2009**, *65*, 148–155, doi:10.1107/S090744490804362X.
82. Macrae, C.F.; Edgington, P.R.; McCabe, P.; Pidcock, E.; Shields, G.P.; Taylor, R.; Towler, M.; van de Streek, J. Mercury : visualization and analysis of crystal structures. *J. Appl. Crystallogr.* **2006**, *39*, 453–457, doi:10.1107/S002188980600731X.
83. Ballantyne, A.D.; Brisdon, A.K.; Dryfe, R.A.W. Immiscible electrolyte systems based on asymmetric hydrophobic room temperature ionic liquids. *Chem. Commun.* **2008**, 4980, doi:10.1039/b809148j.
84. Voloshina, A.D.; Gumerova, S.K.; Sapunova, A.S.; Kulik, N. V.; Mirgorodskaya, A.B.; Kotenko, A.A.; Prokopyeva, T.M.; Mikhailov, V.A.; Zakharova, L.Y.; Sinyashin, O.G. The structure – Activity correlation in the family of dicationic imidazolium surfactants: Antimicrobial properties and cytotoxic effect. *Biochim. Biophys. Acta - Gen. Subj.* **2020**, *1864*, 129728, doi:10.1016/j.bbagen.2020.129728.
85. EC Committee Guidance on Management and Care of Animals Used for Experiments and Other Research Purposes, 2007/526/ EC, of June 18th 2007.
86. *Guide for the Care and Use of Laboratory Animals*; National Academies Press: Washington, D.C., 2011; ISBN 978-0-309-15400-0.
87. *A guide to preclinical drug research. Part One*; Mironov, A.., Ed.; Moscow: Grif and K, 2012.
88. Dye, W.T. Herbicidal alkyl-amino-phosphonium halides U.S. Patent 2774658 1956.
89. Phosphonium Halides and process for the production thereof G.B. Patent 716678 1954.

90. Divinskaya, L.P.; Limanov, V.E.; Skvortsova, E.K.; Putyatina, G.M.; Starkov, A.V.; Grinshtein, N.I.; Nifant'ev, E.E. Search for bactericidal preparations in the series of organophosphorus compounds. *J. Gen. Chem. USSR (Engl. Transl.)* **1966**, *36*, 1244–1246.
91. Pashirova, T.N.; Zueva, I. V.; Petrov, K.A.; Lukashenko, S.S.; Nizameev, I.R.; Kulik, N. V.; Voloshina, A.D.; Almasy, L.; Kadirov, M.K.; Masson, P.; et al. Mixed cationic liposomes for brain delivery of drugs by the intranasal route: The acetylcholinesterase reactivator 2-PAM as encapsulated drug model. *Colloids Surfaces B Biointerfaces* **2018**, *171*, 358–367, doi:10.1016/j.colsurfb.2018.07.049.
92. Pashirova, T.N.; Burilova, E.A.; Tagasheva, R.G.; Zueva, I.V.; Gibadullina, E.M.; Nizameev, I.R.; Sudakov, I.A.; Vyshtakalyuk, A.B.; Voloshina, A.D.; Kadirov, M.K.; et al. Delivery nanosystems based on sterically hindered phenol derivatives containing a quaternary ammonium moiety: Synthesis, cholinesterase inhibition and antioxidant activity. *Chem. Biol. Interact.* **2019**, *310*, 108753, doi:10.1016/j.cbi.2019.108753.
93. Peña-Morán, O.; Villarreal, M.; Álvarez-Berber, L.; Meneses-Acosta, A.; Rodríguez-López, V. Cytotoxicity, Post-Treatment Recovery, and Selectivity Analysis of Naturally Occurring Podophyllotoxins from Bursera fagaroides var. fagaroides on Breast Cancer Cell Lines. *Molecules* **2016**, *21*, 1013, doi:10.3390/molecules21081013.
94. Letai, A. Apoptosis and Cancer. *Annu. Rev. Cancer Biol.* **2017**, *1*, 275–294, doi:10.1146/annurev-cancerbio-050216-121933.
95. Morana, O.; Wood, W.; Gregory, C.D. The Apoptosis Paradox in Cancer. *Int. J. Mol. Sci.* **2022**, *23*, 1328, doi:10.3390/ijms23031328.
96. Ngoi, N.Y.L.; Choong, C.; Lee, J.; Bellot, G.; Wong, A. LA; Goh, B.C.; Pervaiz, S. Targeting Mitochondrial Apoptosis to Overcome Treatment Resistance in Cancer. *Cancers (Basel).* **2020**, *12*, 574, doi:10.3390/cancers12030574.
97. Singh, P.; Lim, B. Targeting Apoptosis in Cancer. *Curr. Oncol. Rep.* **2022**, *24*, 273–284, doi:10.1007/s11912-022-01199-y.
98. Singh, V.; Khurana, A.; Navik, U.; Allawadhi, P.; Bharani, K.K.; Weiskirchen, R. Apoptosis and Pharmacological Therapies for Targeting Thereof for Cancer Therapeutics. *Sci* **2022**, *4*, 15, doi:10.3390/sci4020015.
99. Wang, R.-A.; Li, Q.-L.; Li, Z.-S.; Zheng, P.-J.; Zhang, H.-Z.; Huang, X.-F.; Chi, S.-M.; Yang, A.-G.; Cui, R. Apoptosis drives cancer cells proliferate and metastasize. *J. Cell. Mol. Med.* **2013**, *17*, 205–211, doi:10.1111/j.1582-4934.2012.01663.x.
100. Shoshan-Barmatz, V.; Arif, T.; Shteinfer-Kuzmine, A. Apoptotic proteins with non-apoptotic activity: expression and function in cancer. *Apoptosis* **2023**, *28*, 730–753, doi:10.1007/s10495-023-01835-3.
101. Cetraro, P.; Plaza-Diaz, J.; MacKenzie, A.; Abadía-Molina, F. A Review of the Current Impact of Inhibitors of Apoptosis Proteins and Their Repression in Cancer. *Cancers (Basel).* **2022**, *14*, 1671, doi:10.3390/cancers14071671.
102. Sarsour, E.H.; Kumar, M.G.; Chaudhuri, L.; Kalen, A.L.; Goswami, P.C. Redox Control of the Cell Cycle in Health and Disease. *Antioxid. Redox Signal.* **2009**, *11*, 2985–3011, doi:10.1089/ars.2009.2513.
103. Sadiq, I.Z. Free Radicals and Oxidative Stress: Signaling Mechanisms, Redox Basis for Human Diseases, and Cell Cycle Regulation. *Curr. Mol. Med.* **2023**, *23*, 13–35, doi:10.2174/1566524022666211222161637.
104. Cox, G.; Koteva, K.; Wright, G.D. An unusual class of anthracyclines potentiate Gram-positive antibiotics in intrinsically resistant Gram-negative bacteria. *J. Antimicrob. Chemother.* **2014**, *69*, 1844–1855, doi:10.1093/jac/dku057.
105. Berezovskaya, I.V. Classification of Substances with Respect to Acute Toxicity for Parenteral Administration. *Pharm. Chem. J.* **2003**, *37*, 139–141, doi:10.1023/A:1024586630954.